Open Access

Catalysis Research

LIDSEN Publishing Inc.

Original Research

Novel Microporous Iron(III) Oxide and Silver Oxide *Chomolena odorata* Leaf Biochar Nanocomposite for the Treatment of Well Water

Felix Sunday Nworie [1,*], Chiamaka Mbam [1], Ogonna Ogwa [1], Clinton Oroke [2], Nkechi Eze [1], Chioma Ike-Elechi [1], Collins Chidiebere Igwe [1]

1. Department of Industrial Chemistry, Ebonyi State University, Abakaliki, Nigeria; E-Mails: nworie.sunday@ebsu.edu.ng; mbamchiamaka@gmail.com; virginaog@gmail.com; eze.nkechi@ebsu.edu.ng; chiomaaja@gmail.com; collinsigwe@gmail.com
2. Federal polytechnic Ado-Ekiti, Ekiti State, Nigeria; E-Mail: clintoneo.fpa83@gmail.com

* **Correspondence:** Felix Sunday Nworie; E-Mail: nworie.sunday@ebsu.edu.ng

Academic Editor: Narendra Kumar

Catalysis Research
2026, volume 6, issue 3
doi:10.21926/cr.2603007

Received: April 05, 2026
Accepted: June 14, 2026
Published: July 01, 2026

Abstract

In this study, iron(III) oxide-*Chromolaena odorata* leaf biochar nanocomposite (Fe_2O_3-COLBN) and silver oxide-*Chromolaena odorata* leaf biochar nanocomposite (Ag_2O-COLBN) were prepared and used for the treatment of well water for household use. The fabricated nanocomposites and the pyrolyzed *Chromolena odorata* leaf biochar were characterized using UV-Vis spectroscopy, Scanning Electron Microscopy coupled with Energy Dispersive X-ray spectroscopy (SEM/EDX), X-ray Diffraction (XRD), Fourier Transform Infrared Spectroscopy (FTIR), and Transmission Electron Microscopy (TEM) to elucidate the morphological, structural, and functional properties. The well water was assessed physicochemically and microbiologically using standard procedures and values compared to W.H.O standard. The heavy metal content and antimicrobial effectiveness of biochar and the nanocomposite (as well as biochemical and morphological tests) in the well water were evaluated using atomic absorption spectrophotometry and agar well diffusion method, respectively. Based on the results obtained, Ag_2O-COLBN and Fe_2O_3-COLBN were stable after three-cycle treatment, multifunctional, and microporous, with an average crystallite size of 27-39 nm. Physicochemical data revealed reductions in turbidity, total dissolved solids (TDS), anion

concentrations, and heavy metal concentrations. The antimicrobial assessment showed that 0.001 g each of Ag_2O-COLBN and Fe_2O_3-COLBN inhibited the growth of pathogenic microorganisms in a single 30 min equilibration with 200 cm^3 of well water samples. The nanocomposites (Ag_2O-COLBN and Fe_2O_3-COLBN) are sustainable, low-cost, and efficient materials for well water purification, especially in rural areas, drought-prone areas, and in disaster management environments.

Keywords
Well water; nanocomposites; *Chromolena odorata*; biochar; water purification; antimicrobials

1. Introduction

Well water refers to groundwater that is accessed through a well drilled, dug, or bored into underground aquifers. Well water a primary source of water for drinking, laundry, cooking, and other activities, especially in rural and suburban areas where municipal water supply is unavailable [1]. The quality of well water is influenced by geological formations, depth, and proximity to pollution sources such as septic systems, agricultural runoff, and industrial waste [2]. Although well water can be a reliable source of fresh water, it often requires testing and treatment to ensure it meets safe drinking water standards due to potential contamination from various anthropogenic activities such as agricultural runoff, industrial discharges, and improper waste disposal [3]. These contaminants can introduce heavy metals, pathogenic microorganisms, and organic pollutants into groundwater systems, posing serious health risks to human populations [4].

Owing to these challenges, the development of bio-based nanocomposites has emerged as a promising approach to address the removal of contaminants. These materials offer the combined advantages of high surface area, chemical reactivity, and environmentally benign properties that conventional water purification methods do not [5]. Among various biomass sources, *Chromolaena odorata*, commonly known as Siam weed, has attracted much attention for its widespread availability, high lignocellulosic content, and phytoremediative potential [5]. The selection of *Chromolaena odorata* as the precursor biomass is particularly strategic due to its abundance and invasiveness across tropical regions such as sub-Saharan Africa and Southeast Asia [6]. Utilizing this weed for nanocomposite production addresses environmental concerns associated with its proliferation while providing a renewable and low-cost feedstock for biochar synthesis. Furthermore, the plant's phytochemical constituents such as phenolics, flavonoids, and alkaloids can influence the surface chemistry of the resulting biochar, potentially enhancing its interaction with metal oxides and target contaminants [7]. Transforming this invasive plant species into value-added products of biochar and subsequent fabrication of nanocomposites not only addresses environmental pollution but also adds economic value to waste biomass.

Biochar, a carbon-rich product derived from the pyrolysis of organic biomass under limited-oxygen conditions, has demonstrated potential in water treatment applications due to its porosity, surface functional groups, and ion exchange capabilities [8]. However, the adsorption efficiency of pristine biochar can be limited by its surface chemistry and the nature of target pollutants. To enhance its functionality, biochar can be modified with metal oxide nanoparticles such as iron(III)

oxide (Fe_2O_3) and silver oxide (Ag_2O), forming nanocomposites with superior physicochemical and antimicrobial properties.

Iron(III) oxide nanoparticles are particularly effective for removing heavy metals and anionic pollutants through adsorption, redox reactions, and catalytic degradation mechanisms [9]. They offer high affinity for arsenate, phosphate, and fluoride ions, and are known for their low toxicity and environmental friendliness. When incorporated into a biochar matrix, Fe_2O_3 nanoparticles can increase surface area, introduce active binding sites, and enhance overall pollutant-removal capacity [10].

Silver oxide nanoparticles, on the other hand, are well-recognized for their potent antimicrobial properties, attributable to their ability to disrupt microbial cell membranes, generate reactive oxygen species (ROS), and interfere with enzymatic functions [11]. Additionally, Ag_2O nanoparticles exhibit photocatalytic activity, enabling the degradation of organic pollutants under light irradiation. When supported on a biochar platform, silver oxide enhances both the adsorptive and antimicrobial capabilities of the composite, making it suitable for treating water contaminated with biological and chemical agents.

Therefore, Fe_2O_3 and Ag_2O nanoparticles on a *Chromolaena odorata* biochar matrix could result in a multifunctional nanocomposite with synergistic properties for water purification. Such a hybrid material would leverage the adsorption potential of iron oxide, the antimicrobial and photocatalytic properties of silver oxide, and the structural support and surface functionality of biochar. The integration of these components aims to develop a low-cost, sustainable, and efficient material for point-of-use water treatment, especially in rural and peri-urban communities where centralized treatment infrastructure is lacking.

Previous studies have demonstrated the feasibility of using metal-oxide-modified biochars for water remediation [12]. It was reported that Fe-modified biochar derived from corn straw effectively removed heavy metals such as Pb^{2+} and Cd^{2+} from aqueous solutions [12]. Similarly, Ag-loaded biochars that exhibited significant antibacterial activity against *Escherichia coli* and *Staphylococcus aureus*, along with enhanced dye adsorption capabilities, have been reported [13-16].

The treatment of well water using Fe_2O_3 and Ag_2O-*Chromolaena odorata* biochar nanocomposite is expected to improve water quality parameters, including reductions in turbidity, microbial load, and concentrations of toxic ions or organic dyes. These outcomes are particularly relevant in light of global efforts to achieve Sustainable Development Goal 6 (clean water and sanitation), which emphasizes universal access to safe and affordable drinking water [17]. Moreover, the use of such low-cost, easily deployable materials could significantly reduce the burden on existing water supply systems, especially in emergency or low-resource settings.

The objectives of the study were to evaluate the practical potential of the synthesized nanocomposite and to use various characterization techniques such as Fourier Transform Infrared Spectroscopy (FTIR), Scanning Electron Microscopy (SEM), Energy Dispersive X-ray Spectroscopy (EDX), X-ray Diffraction (XRD), and Transmission Emission Microscopy (TEM); surface area analysis has been employed. These methods provide insights into the structural, morphological, and chemical properties of the nanocomposites, and correlate them with their performance in water treatment. Batch adsorption studies and antimicrobial assays were used in assessing the efficacy of the nanocomposite under ambient environmental conditions.

Therefore, the development and evaluation of iron(III) oxide and silver oxide-*Chromolaena odorata* biochar nanocomposites represent a novel and promising approach to decentralized water purification. This research aligns with the global movement toward green nanotechnology, sustainable resource utilization, and environmental stewardship. By transforming an invasive plant into a multifunctional water-treatment material, the study offers a practical pathway to improving water security in underdeveloped regions, while contributing to waste valorization and pollution mitigation efforts.

2. Materials and Methods

2.1 Materials

2.1.1 Equipment and Instruments

Instrumentation.

Instrumentation for the structural, morphologicaland elemental composition of the Chromolena odorata leaf biochar (COLB) and the nanocomposites was done using standard analytical procedures. Genesis 10S UV-Vis spectrophotometer was used to determine the UV-Vis spectra. The Bruker® D8 Discover x-ray diffractometer, equipped with a Lynx Eye detector, under Cu-Ka radiation (λ = 1.5406 Å at 40 KV and at 30 mA) was used for the determination of the crystalline nature of the COLB and nanocomposite and diffraction recorded with 2θ = 10 to 70. Phenom Prox by Phenom World, Eindhoven, Netherlands, was applied for the determination of the structural morphology of the COLB and nanocomposite. The Cary 630 Agilent Technologies, USA, Fourier transform infrared spectrophotometer (Shimadzu, Japan) in the range of 4000–400 cm^{-1} in KBr using nujol mull as the mulling agent was used for functional group determination. The TEM analysis for determining the average crystallite size was done using a JEM ARM 200F. Physicochemical analysis involving temperature, salinity, pH, total hardness, dissolved oxygen, electrical conductivity was effected using Smart 6-in-1 pH multimeter. All drying and equilibrations were effected using oven (model DHG) and rotary shaker (RF-12 Remi equipment) respectively. The Erlenmeyer flask, Autoclave (Alpha Laboratory, Ltd) model NL280-A, Pressure Cooker (Crown Star Atsago, India Instruments Pvt Ltd., India and water bath (helmreasinn multipurpose) model DK420, incubator, and microscope were used for antimicrobial experiments. All microbiological weighing was executed using an analytical balance, Mettler Toledo PL, 303.

Reagents.

Analytical grade reagents were sourced from Merck Germany, Biolbs M0270, England, Zymo Research, Promega Madison, WI, USA, BioRad Universal Hood II Philadelphia, PA, USA, NZYtech Lisbon, Portugal, and K.J. Pharmaceutical and chemical and used without further modification: The following reagents were used for the synthesis of the nanocomposite and for well water tests. Iron(III) trioxonitrate(V), Silver trioxonitrate(V), hydrochloric acid, potassium heptaoxodichromate(VI), ethanol, tetramethyl-p-phenylenediamine, crystal violet, lugols Iodine, acetone, safranin, hydrogen peroxide, dimethylsulphoxide, ethanol, barium chloride, concentrated sulphuric acid, alpha-naphthol (Barrit's solution A), phenol disulphonic acid, tetraoxosulphate(VI) acid, barium chloride, Potassium hydroxide, (Barrit's solution B), Zr Fungal/Bacterial DNA Miniprep, Agarose powder, Nuclease free water, Taq 2× Master Mix, UV transilluminator, molecular weight

ladder, Eosin methylene blue agar, *Salmonella and Shigella* agar, MacConkey agar, Bushnel-Hans agar, Sabraud Dextrose agar and Simmon citrate agar.

2.2 Collection, Identification and Preparation of Chromolena odorata Leaf Extract

The Leaves of *Chromolena odorata* were collected from a farmland in Ebonyi State University, Abakaliki, as identified by a specialist botanist from the Department of Applied Biology, Ebonyi State University, Abakaliki. The leaves were washed several times with distilled water and then dried in open air for one week. The leaves were ground into fine powder and kept in a container. The extract of *Chromolena odorata* leaves was prepared by measuring 10 g of ground leaves into 200 cm3 of distilled water, then stirring and heating at a temperature of 80°C for 30 min in a water bath. The *Chromolena odorata* leaf extract (COLE) obtained was allowed to cool, filtered, and the filtrate used for the preparation of the nanocomposite.

2.2.1 Preparation of *Chromolena odorata* Leaf Biochar

Chromolena odorata leaf biochar (COLB) was prepared from the dried leaves of *Chromolena odorata* by carbonization. Consequently, 600 g of dried leaves were loaded into a carbonizer and the temperature was set at 400°C for 30 min. The formed COLB was collected, ground into fine powder, and kept in an airtight container.

2.2.2 Preparation of Silver Oxide and Iron(III) Oxide *Chromolena odorata* Leaf Biochar Nanocompopsite

The synthesis of the nanocomposites involves the addition of 0.3 g each of silver trioxonitrate(V) or iron(III) trioxonitrate(V) for silver oxide and iron(III) oxide *Chromolena odorata* leaf biochar nanocomposite respectively to two separate conical flasks. Then, 10 g of COLB and 100 cm^3 of *Chromolena odorata* leaf extract were added separately to a 1000 cm^3 distilled water in each flask. The mixture was heated with continuous stirring for 30 min and then cooled and centrifuged at 4000 rpm. The formed nanocomposites (iron(III) oxide *Chromolena odorata* leaf biochar nanocomposite (Fe_2O_3-COLBN) and silver oxide *Chromolena odorata* leaf biochar nanocomposite (Ag_2O-COLBN)) were collected, washed with ethanol and distilled water to pH 7, dried at a temperature of 110°C for 2 h, and then kept for further use in an airtight container.

2.2.3 Collection and On-Site Treatment and Physicochemical Analysis of Well Water Samples

Standard analytical protocols were used to sample well water samples early in the morning (between 7 and 10 a.m.) from different locations (Figure 1) using plastic bottlesprewashed with dilute trioxonitrate(V) acid. Two containers were used for each sampling point, with one container treated with two drops of acid to prevent oxidation before heavy metal determination [18]. The well was allowed to run for at least ten min before assaying the samples. Physicochemical parameters were taken in situ at the sampling site and in the laboratory using standard analytical instruments. The water samples were then transported to the chemistry and microbiology laboratory in sterile bottles for further analysis (heavy metal, physicochemical, and antimicrobial tests).

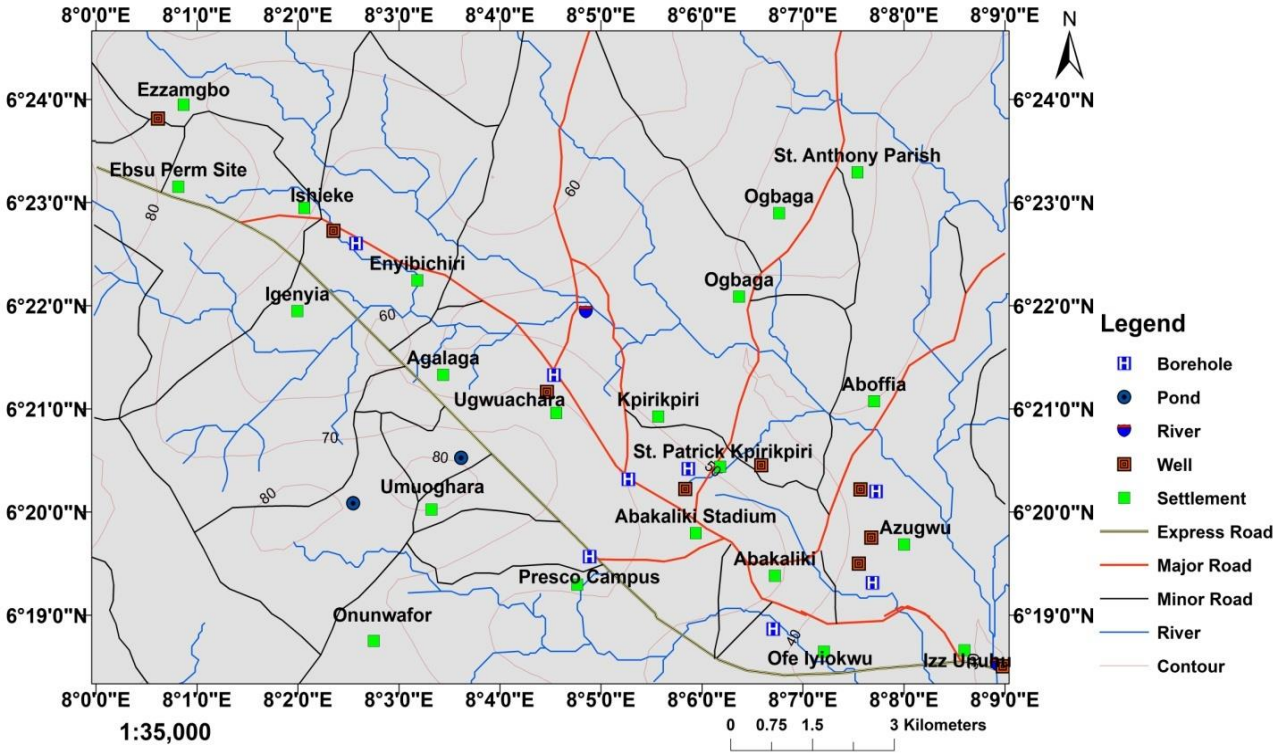

Figure 1 Map of the study area.

In the treatment of the well water samples, 200 cm^3 of each sample was measured and added to a sterile, labeled, separate container foreach nanocomposite. Then 0.5 g of Fe_2O_3-COLBN or Ag_2O-COLBN was added, and the mixture was equilibrated for 30 min at 27°C. The mixture was filtered as described elsewhere [18], and the filtrate was kept for further analysis.

2.2.4 Recovery Studies

The nanocomposites were desorbed with HCl, washed with distilled water, dried, and reused three times to evaluate the stability.

2.2.5 Heavy Metal, Chloride, Sulphate and Nitrate Determination

The concentrations of heavy metals in the well water before and after treatment with the nanocomposites were determined using the atomic absorption spectrophotometric method [19]. The concentrations of the anions (Cl^-, SO_4^{2-} and NO_3^-) present in the water samples before and after treatment with nanocomposites were also determined using standard procedures as described elsewhere [20].

2.2.6 Antimicrobial Evaluation of the COLB, Fe_2O_3-COLBN, Ag_2O-COLBN

The agar well diffusion method as described elsewhere [21] was used to determine the antimicrobial efficacy of the COLB, Fe_2O_3-COLBN, and Ag_2O-COLBN. The test Organisms; *Staphylococcus aureus*, *Escherichia coli*, *Klebsiella*, *Salmonella spp.*, *Candida albicans*, *Aspergillus* and *proteus* were tested for. The isolates were accessed from Alex Ekwueme Federal Teaching Hospital, Abakaliki, Nigeria, and then carefully transported in nutrient broth to the Ultra Modern

Laboratory of the Department of Applied Microbiology, Ebonyi State University, Abakaliki. The antimicrobial inhibitory test was performed on different concentrations (0.001, 0.01 and 0.1 g) of the COLB, Fe_2O_3-COLBN, and Ag_2O-COLBN against the test organisms by dissolving the COLB, Fe_2O_3-COLBN, and Ag_2O-COLBN in dimethylsulfoxide [22]. During the test, the cultures of the test organisms were made in nutrient broth, incubated for 24 h, and adjusted to the McFarland turbidity standard. The blank control (gentamycin for bacteria and amphotericin β for fungi) were prepared and aseptically deposited on the Mueller-Hinton agar plates. Then, the cultures of the test organisms and controls were incubated at 37°C for 18-24 h, and the inhibition zone diameters were measured according to standard protocols.

2.2.7 Antimicrobial Evaluation of the Water Samples

Different media such as Cetrimide agar*, Salmonella*/*Shigella* agar, Eosin Methylene Blue agar, Macconkey agar, Nutrient agar, Sabraud Dextrose agar and Bushnel-Hans agar were made for the antimicrobial evaluation of the water samples and were prepared according to the manufacturers instruction. Sterile containers of 500 cm^3 was used to transport the water samples at a temperature of 8°C to Ultra-Modern Laboratory of Ebonyi State University, Abakaliki, Nigeria and all were processed within 6 h after collection. All the tests were executed as described elsewhere without modification [6].

2.2.8 Isolation and Identification of Bacterial Strains (Biochemical and Morphological Studies)

The isolation and identification of bacterial strains (Gram staining, cell arrangement, indole test, oxidase test, catalase test, coagulase test, citrate test, and methyl red test) were done using standard procedures as described elsewhere [23, 24]. The coliform count per unit (CFU/mL) was determined using Equation 1.

$$\frac{CFU}{mL} = \frac{number\ of\ colony}{volume\ of\ water} \times dilution\ factor\ (10^3) \quad (1)$$

3. Results and Discussion

3.1 Physicochemical Properties of Initial Water Samples

The Physicochemical properties of well water before treatment with nanocomposites show various parameters of water quality from multiple wells. These parameters include pH, total hardness, resistivity, salinity, total dissolved solids (TDS), and electrical conductivity, all of which are critical indicators of water suitability for domestic or industrial use. The pH, a measure of the hydrogen ion concentration, for ideal drinking water is between 6.5 and 8.5 [25]. Based on Figure 2, the pH values across the wells are within an acceptable range, suggesting that the water is neither too acidic nor too basic before treatment. Total hardness, largely due to the presence of calcium and magnesium ions, affects the suitability of water for washing and taste. Several wells, such as Omege junction well and Best care hospital well (Figure 2), show relatively high total hardness, indicating potential scaling issues and aesthetic concerns, as the values are above 150 ppm [26].

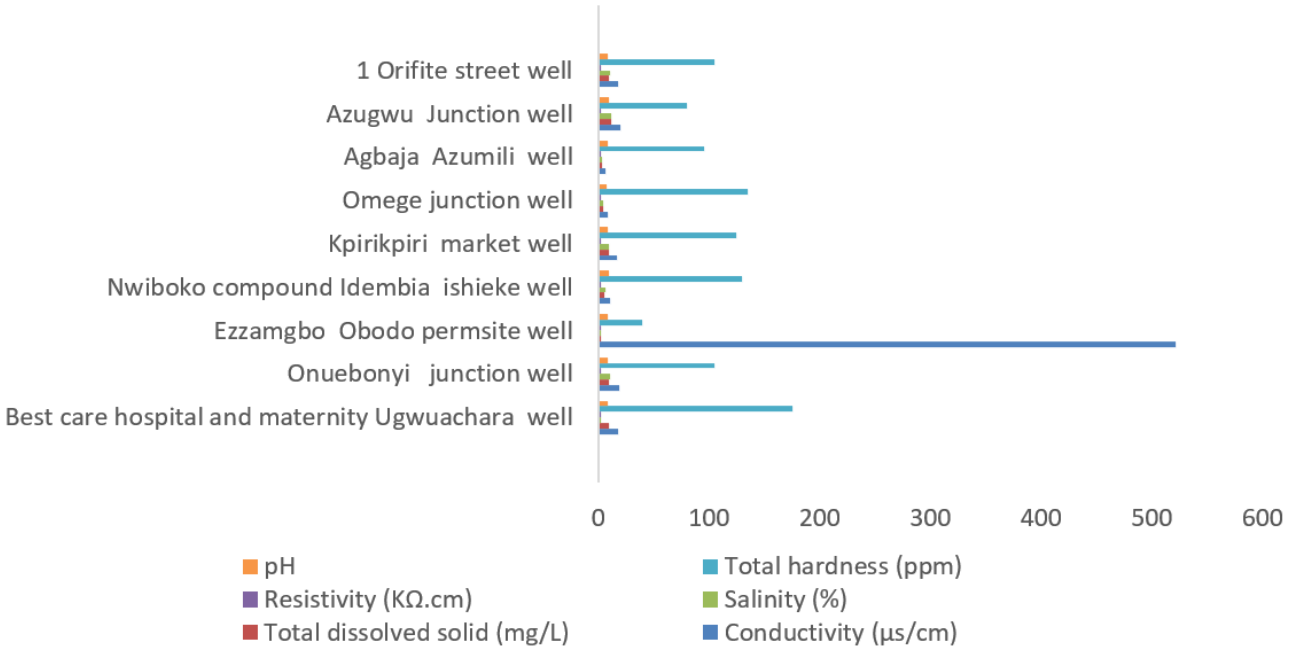

Figure 2 Physicochemical properties of well water before treatment with nanocomposites.

Resistivity, an indicator of the ionic purity of the water, indicates that some well water samples have low resistivity, suggesting higher ionic concentration and possible contamination, as shown in Figure 2. Figure 2 clearly shows low resistivity values in most wells, especially in the Ezzangbo Obodo perm site well, indicating possible ionic or heavy-metal contamination as noted elsewhere [27]. Salinity, a measure of dissolved salt concentration, is relatively low in most samples, as shown in Figure 2. Studies have shown that elevated salinity can affect taste and health, and chronic exposure to saline water can lead to hypertension and other health issues [25]. The TDS comprises both organic and inorganic substances and is moderately high in most of the well water samples, as shown in Figure 2. According to WHO (2017) [28], TDS levels above 500 mg/L are generally considered unsuitable for drinking and most of the well water are above this level and therefore needs purification before human consumption. Conductivity relates directly to the presence of ions in water and is a useful measure of overall water quality. High conductivity values were particularly observed in Ezzangbo Obodo perm site well water (600 µS/cm), indicating high levels of dissolved ions, which may correlate with pollution or intrusion of waste or mineral-rich sources [26]. Based on the analysis, the physicochemical properties of many wells show values that may raise concern, particularly regarding total hardness, conductivity, and TDS. These parameters, if unchecked, could pose serious health risks and indicate contamination from geogenic or anthropogenic sources. Consequently, the application of biogenic nanocomposite treatment is justified to improve the quality of these well water samples.

Figure 3 presents the effects of treatment with silver-*Chromolaena odorata* leaf biochar nanocomposite (Ag-COLBN) on the physicochemical properties of well water from various locations. The parameters measured include pH, total hardness (ppm), resistivity (KΩ·cm), salinity (%), total dissolved solids (mg/L), and conductivity (µS/cm). The pH values across all well water samples are within a narrow range, indicating neutral to alkaline conditions, which fall within the acceptable limits for potable water [26]. There is a significant reduction in total hardness as observed in some

samples, with the highest values in wells such as Kpirikpiri market well and Best Care Hospital well. Silver biochar likely contributes to ion exchange or precipitation of hardness-causing ions such as Ca^{2+} and Mg^{2+} [27]. Post-treatment values indicate improved resistivity in certain wells, which corresponds to reduced ionic content. The salinity values are consistently low across all samples, indicating that Ag-COLBN treatment maintains low salinity, highlighting its efficiency in removing excess salts without adding new ions. The TDS levels vary but are significantly lower in samples like Agbaja Azumili well and Onuebonyi junction well, indicating effective removal of soluble impurities through adsorption of heavy metals and organic matter [26]. High conductivity observed in Ezzamgbo Obodo perm site well and Nwiboko compound Idembia well water samples suggests a higher concentration of ionic species, possibly due to partial treatment or location-based variation in contamination. Silver-loaded *Chromolaena odorata* biochar (Ag-COLBN) demonstrates efficacy in altering the physicochemical profile of well water, as its adsorptive and catalytic surface helps to trap and degrade pollutants, aligning with sustainable water treatment goals.

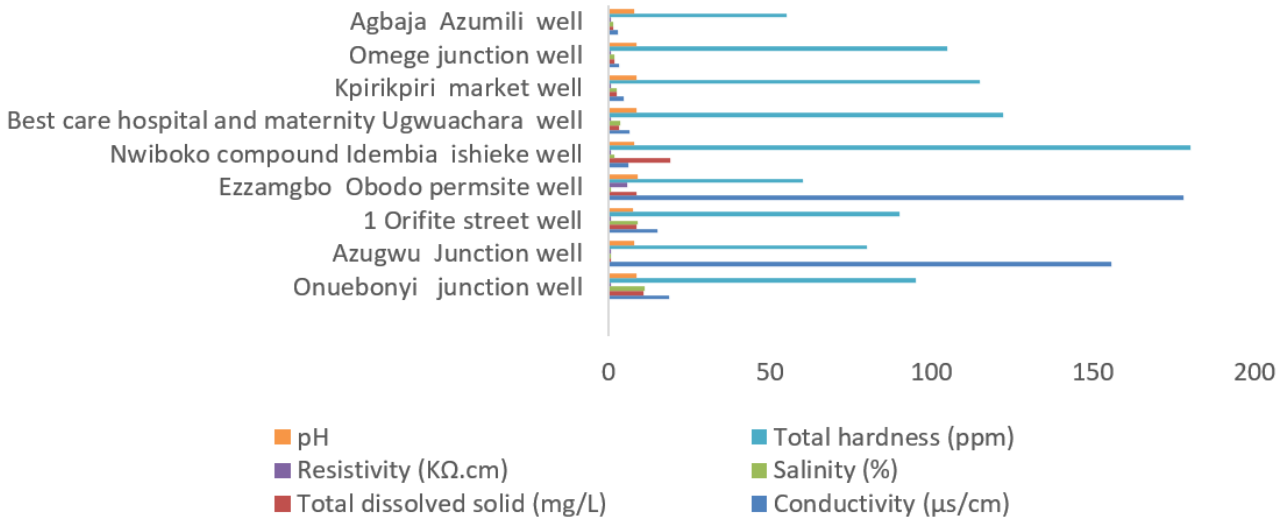

Figure 3 Physicochemical properties of silver oxide nanocomposite treated well water (Ag-NCTWW).

Figure 4 presents data on several physicochemical parameters of treated well water using iron(III) oxide nanocomposite. The pH levels across all treated wells are slightly neutral to alkaline, indicating effective moderation by the nanocomposite, and this aligns with findings [29], who noted that iron-based nanocomposites can buffer pH within acceptable WHO ranges (6.5-8.5) after treatment. The hardness levels in all water samples are substantially reduced, with all values below 150, demonstrating the nanocomposite's capacity to reduce calcium and magnesium concentrations through ion exchange and precipitation [26]. Higher resistivity values in some samples indicate a reduction in ionic content post-treatment and a corresponding decrease in conductivity, suggesting effective deionization by the nanocomposite [26]. Salinity remains low across the board, indicating that the iron(III) oxide nanocomposite treatment does not introduce excessive salts and may help remove existing saline content, confirming the adsorptive potential of the nanocomposite [27]. The TDS values are significantly reduced in most wells, except for a notable spike in the Ezzamgbo Obodo Permsite Well water though below 500 mg/L acceptable for WHO (2017) [28], suggesting possible leaching or localized contamination despite treatment. Most samples have conductivity under 250

µS/cm except for Ezzamgbo Obodo Permsite Well water, which shows an unusually high value (~550 µS/cm). This could be due to poor retention or excessive ions remaining after treatment [25].

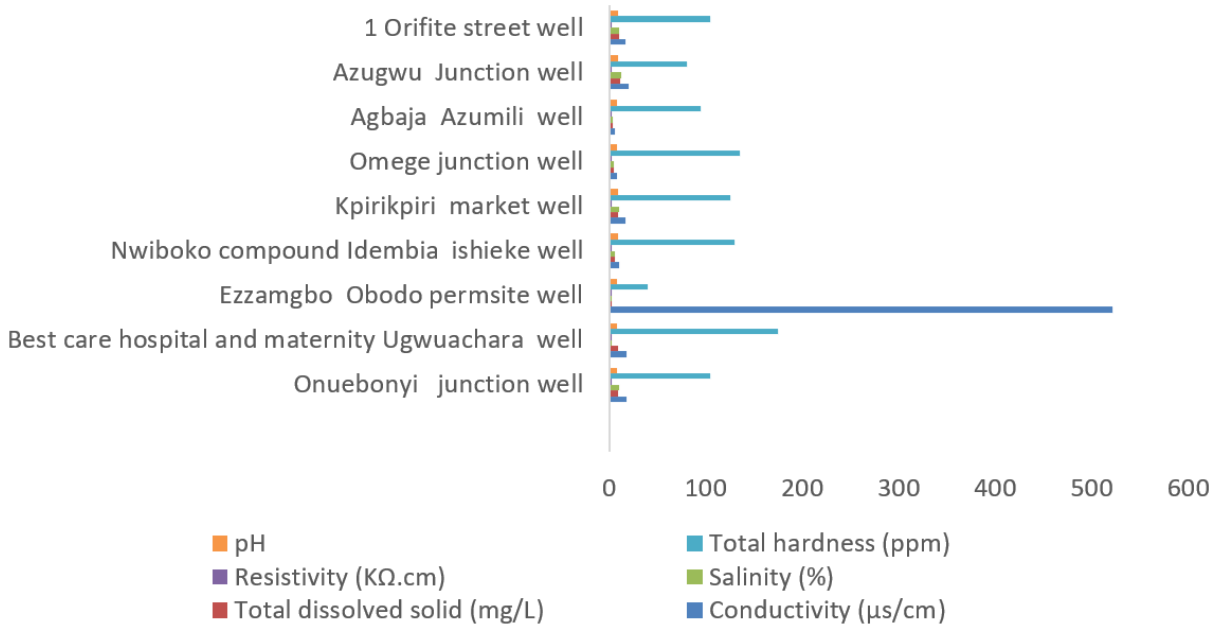

Figure 4 Physicochemical properties of Fe-NCTWW (iron(III) oxide nanocomposite treated well water).

3.2 Heavy Metals in Well Water

Common heavy metals assessed include lead (Pb), cadmium (Cd), chromium (Cr), iron (Fe), zinc (Zn), copper (Cu), and manganese (Mn). Figure 5 shows concentrations of heavy metals in untreated well water. In most samples, concentrations of lead (Pb), cadmium (Cd), and iron (Fe) were above the permissible limits recommended by the World Health Organization (WHO, 2017) [28].

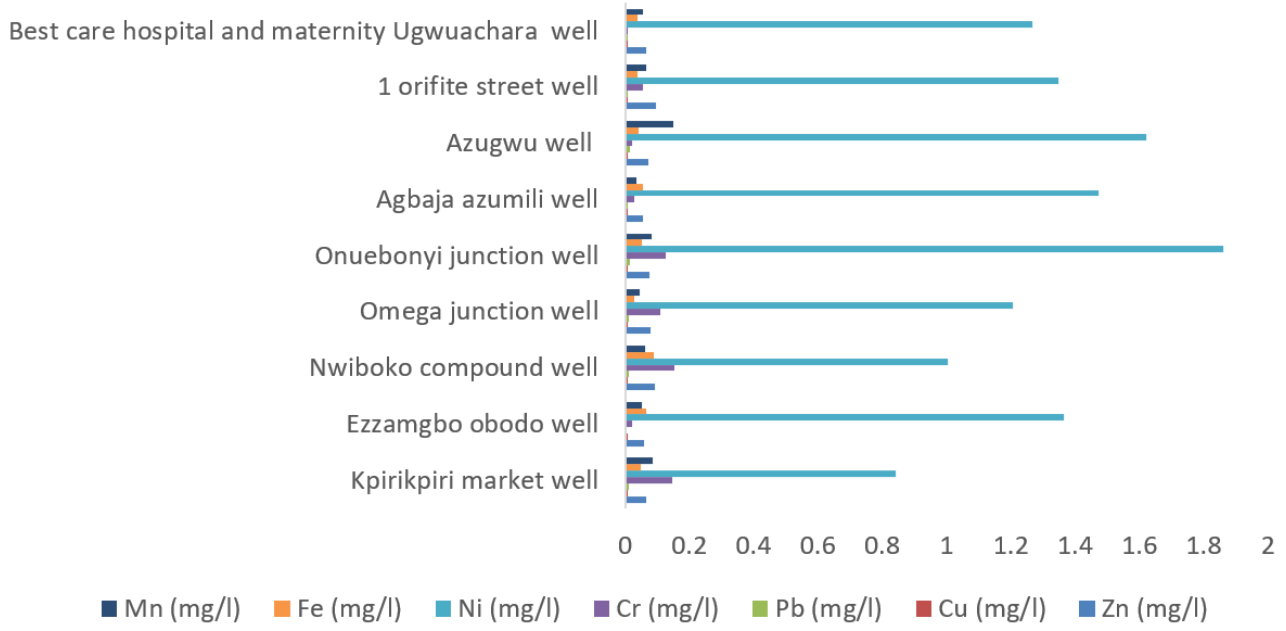

Figure 5 Heavy metals in well water samples before treatment.

Lead (Pb) was observed at concentrations up to 0.12 mg/L, exceeding the WHO guideline of 0.01 mg/L. Lead exposure in drinking water is associated with neurotoxicity, especially in children [28]. The likely sources of lead contamination include corroded plumbing, industrial activities, or runoff from nearby waste disposal sites. Cadmium (Cd) was detected at 0.02 mg/L, above the WHO limit of 0.003 mg/L. Cadmium is a known carcinogen, and its presence in groundwater is often due to agricultural runoff or improper disposal of electronic waste [28]. Iron (Fe) levels, reaching 1.8 mg/L, surpass the SON permissible limit of 0.3 mg/L [29]. Though iron is essential in small amounts, excessive concentrations can cause water staining of laundry and contribute to microbial growth [26]. Zinc (Zn) and copper (Cu) were generally within acceptable limits, indicating minimal contamination from industrial or household plumbing sources. Chromium (Cr), detected at 0.08 mg/L, is slightly above the WHO permissible limit of 0.05 mg/L in some samples. Hexavalent chromium is toxic and linked to liver and kidney damage. Manganese (Mn)was found above 0.4 mg/L and also exceeded the WHO guideline of 0.1 mg/L, possibly due to natural leaching from rocks or old steel pipes.

Figure 6 shows the heavy metals in well water samples after treatment with iron(III) oxide-*Chromolaena odorata* leaf biochar nanocomposite and Silver oxide-*Chromolaena odorata* leaf biochar nanocomposite. Both nanocomposites demonstrated significant reductions in heavy metal concentrations. The Pb and Cd levels were substantially reduced, often below WHO permissible limits of 0.01 mg/L and 0.003 mg/L, respectively [28]. The Zn and Cu, which are essential micronutrients but toxic at high doses, were also efficiently removed to safe levels, as indicated in Figure 6. Iron and Mn, which are common in groundwater, showed high adsorption efficiency likely due to the affinity of multifunctional groups on the nanocomposite for divalent ions [27]. The Ag-COLBN showed slightly higher removal efficiency across most metals, possibly due to the enhanced surface reactivity and antibacterial synergy of silver, which also prevents biofouling during the treatment process [30]. The Fe_2O_3-COLBN was more effective in the removal of iron and manganese, likely due to ion exchange and redox reactions catalyzed by Fe^{3+} in the composite. The removal of heavy metals can be attributed to adsorption or ion exchange between metal and surface functionalities such as -OH, -COOH), complexation and precipitation.

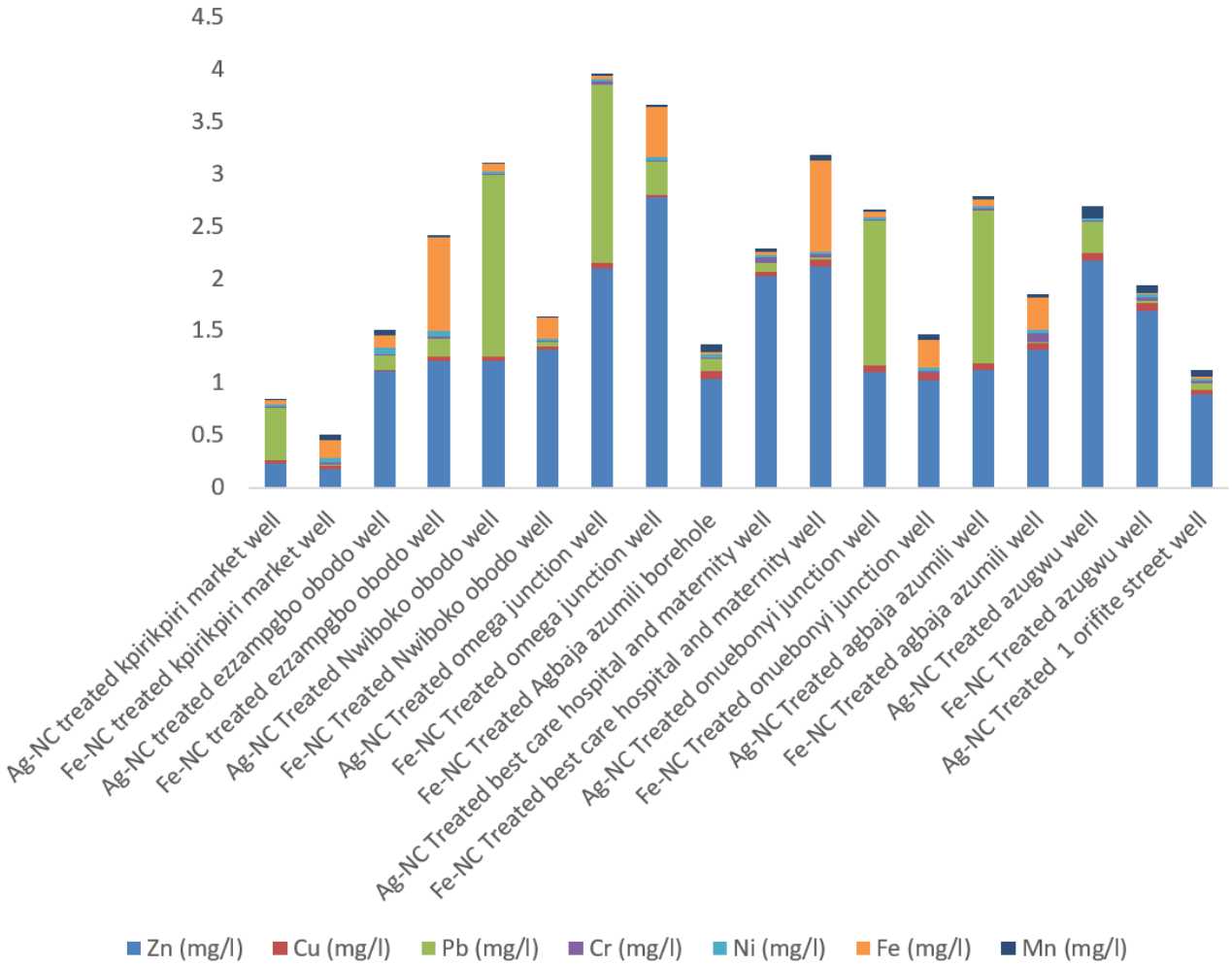

Figure 6 Heavy metals in well water samples after treatment with Fe_2O_3-COLBN and Ag_2O-COLBN.

3.3 Anions in Well Water Samples Before Treatment

The chloride (Cl^-), nitrate (NO_3^-), and sulfate (SO_4^{2-}) are commonly analyzed in water quality assessments due to their significant impacts on human health and environmental quality. These anions are common contaminants in groundwater, often resulting from agricultural runoff, domestic sewage, and natural geochemical processes.

In the analyzed well water samples, the concentrations of most anions remained within WHO [28] permissible limits, as shown in Figure 7, indicating minimal contamination, whereas some are above the limits. Elevated nitrate ion levels in untreated samples may pose a risk of methemoglobinemia (blue baby syndrome) in infants and other health concerns [2].

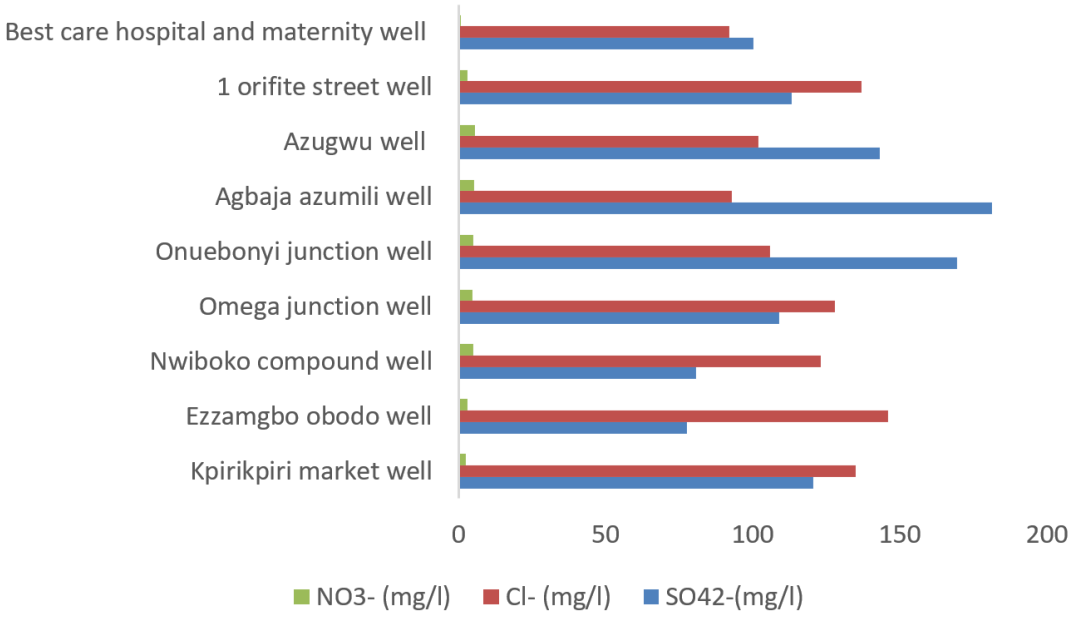

Figure 7 Anions in well water samples before treatment.

3.4 Anions in Well Water Samples after Treatment with Ag-COLBN and Fe-COLBN

The treatment of well water samples using Ag-COLBN and Fe-COLBN showed a significant reduction in the concentrations of nitrate (NO_3^-), sulfate (SO_4^{2-}), and chloride (Cl^-) as shown in Figure 8 and Figure 9. After treatment, the concentrations of these anions were observed to fall within the permissible limits set by the WHO, 2017 [28] and the Nigerian Standard for Drinking Water Quality [2]. The Ag-COLBN and Fe-COLBN significantly reduced nitrate levels, possibly through adsorption onto the porous surface of the biochar and redox interactions facilitated by silver oxide, which may promote denitrification [30]. High concentrations of sulfate ions can cause laxative effects and a bitter taste. Post-treatment values indicated a reduction in sulfate levels, likely due to the adsorption affinity of biochar for anionic species through surface functional groups like hydroxyls and carboxyls [30]. Chloride, which can corrode metal pipes and impact taste, was reduced effectively by the nanocomposite, suggesting ionic exchange and electrostatic interactions between Ag^+ or Fe^{3+} and Cl^- on the biochar surface.

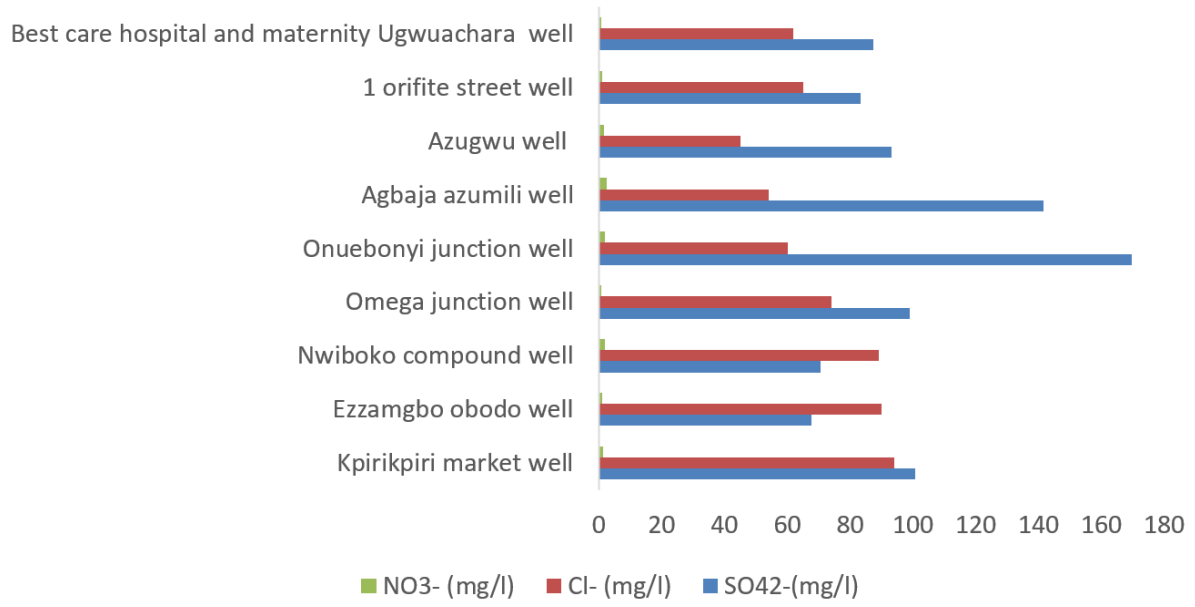

Figure 8 Anion concentration of Ag-COLBN treated well water.

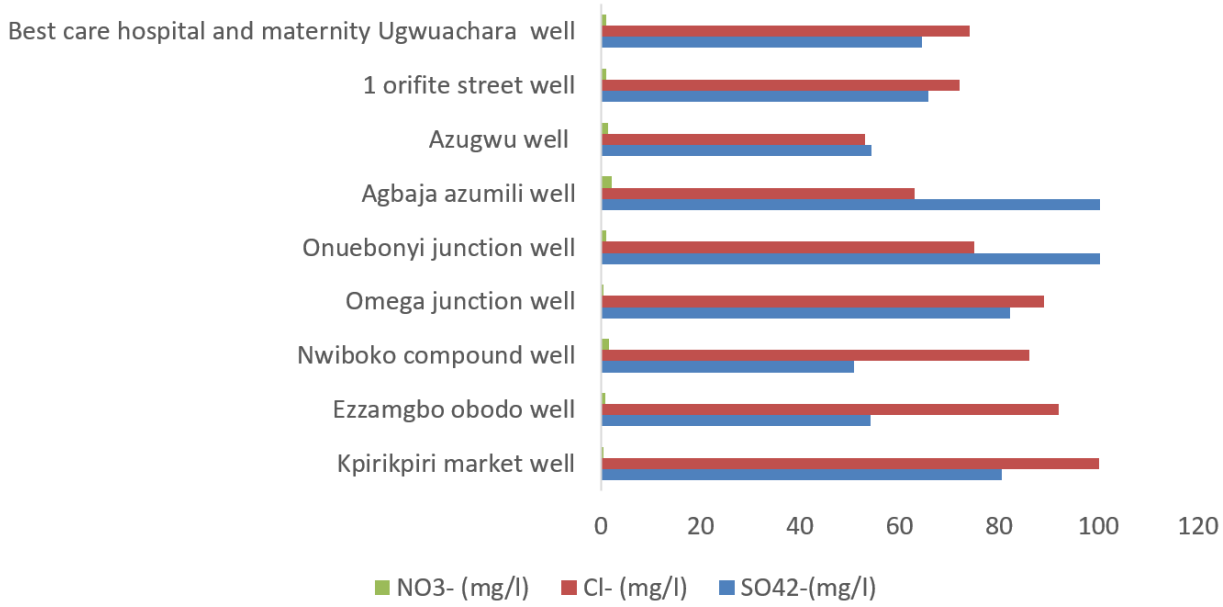

Figure 9 Anion concentration of Fe-COLBN treated well water.

3.5 Optimization of Adsorption Parameters and Evaluation of Adsorption Capacity of Nanocomposites

3.5.1 Effect of Operational Parameters on Heavy Metal Removal

The influence of nanocomposite dosage, pH, and contact time on the percentage removal of heavy metals from borehole water is presented in Figure 10 The removal efficiency increased progressively with increasing adsorbent dosage up to 0.5 g. Beyond this optimum dosage, only marginal improvements were observed, suggesting possible active-site saturation and/or particle aggregation that limit further adsorption efficiency [7].

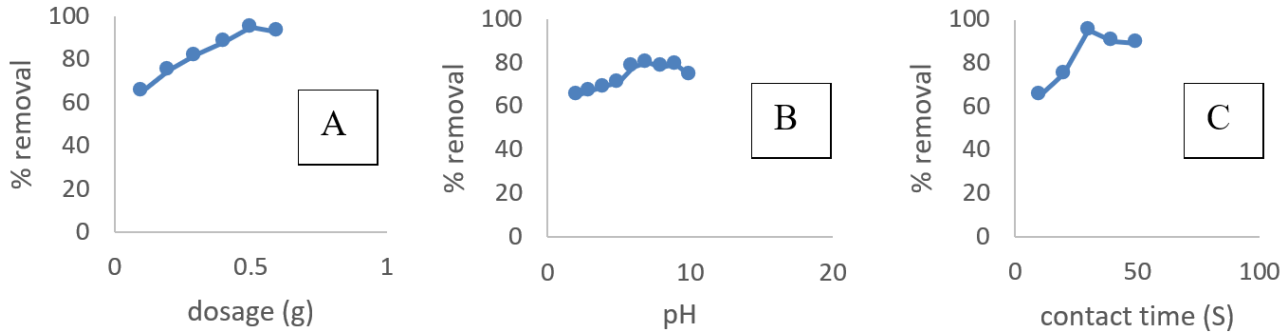

Figure 10 Effect of Nanocomposite dosage (A), pH (B), and contact time (C) on percentage removal of heavy metals from borehole water.

The effect of pH (Figure 10) showed a gradual increase in removal efficiency from acidic to near-neutral conditions, with maximum performance observed at neutral to slightly alkaline pH. This behavior indicates favorable surface charge interactions under these conditions and reduced competition between hydrogen ions (H^+) and metal cations for adsorption sites [30].

Similarly, contact time significantly influenced adsorption performance. The removal efficiency increased rapidly with increasing contact time, reaching equilibrium at approximately 30 minutes. Beyond this point, a slight decline was observed, indicating possible desorption or redistribution of adsorbed species on the nanocomposite surface.

3.5.2 Adsorption Capacity Evaluation

The adsorption capacity (q_e) of the nanocomposites for heavy metal removal was determined using the mass balance equation:

$$q_e = \frac{(C_i - C_f) \times \mathrm{V}}{M} \tag{2}$$

where q_e represents the adsorption capacity (mg/g), C_i is the initial metal concentration (mg/L), C_f is the equilibrium concentration after treatment (mg/L), V is the volume of the solution (L), and M is the mass of the adsorbent (g) [6].

In this study, 0.5 g of Fe_2O_3-COLBN or Ag_2O-COLBN nanocomposite was introduced into 200 cm^3 (0.2 L) of borehole water and equilibrated for 30 minutes at 27°C. Following filtration, the residual metal concentrations were measured and used to compute q_e, thereby quantifying the adsorption performance under the defined experimental conditions.

The adsorption system exhibited a typical dosage-dependent behavior, where increasing adsorbent mass enhanced removal efficiency due to the greater availability of active surface sites. However, adsorption capacity (mg/g) decreased with increasing dosage, reflecting reduced adsorbate loading per unit mass of adsorbent. The maximum adsorption capacity of 650 mg g^{-1} observed at 0.1 g highlights highly efficient adsorbate-adsorbent interactions at low dosage, consistent with adsorption behavior commonly reported for nanostructured materials [30].

3.6 Reusability and Stability of the Nanocomposites

3.6.1 Reusability Performance Over Successive Cycles

The reusability of the nanocomposites was evaluated over three consecutive adsorption-desorption cycles to assess operational stability and regeneration efficiency. After each cycle, the spent adsorbent (0.5 g) was regenerated using 0.01 M HCl, thoroughly washed with deionized water until neutral pH was attained, dried, and reused under identical experimental conditions to treat200 cm^3 of borehole water.

As shown in Figure 11, the removal efficiency declined slightly across successive cycles. The efficiencies recorded were 95.0 ± 0.8%, 94.0 ± 1.0%, and 93.0 ± 1.2% for the first, second, and third cycles, respectively. Despite this marginal decrease, the nanocomposites retained approximately 97% of their initial performance after three cycles, corresponding to a total efficiency loss of about 3%. Importantly, no statistically significant variation in decontamination efficiency across cycles was observed, indicating consistent adsorption performance. The narrow error margins further confirm the reproducibility and structural stability of the nanocomposites during repeated use [6]. Such stability is essential for practical water treatment applications, where adsorbent durability directly influences process economics and sustainability [7].

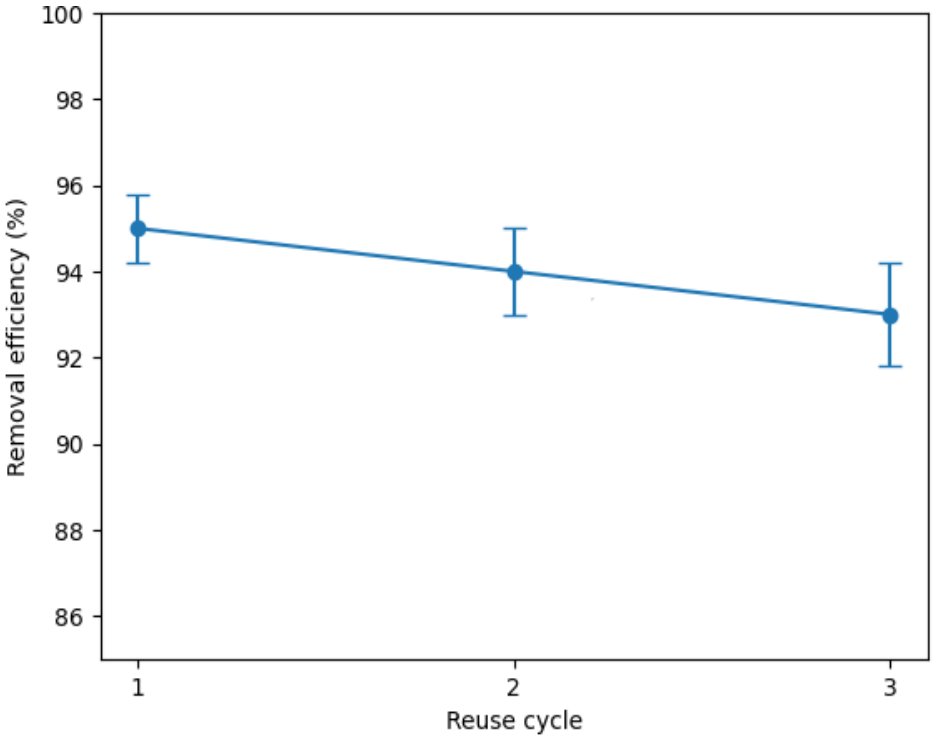

Figure 11 Reusability of nanocomposite over successive treatment cycles.

3.6.2 Stability Mechanism During Regeneration

The observed high reusability is attributed to the structural integrity of the nanocomposite matrix and the reversible nature of adsorption processes. Acid regeneration with dilute HCl protonates surface functional groups (-OH, -COOH, and $-NH_2$), facilitating desorption of bound metal ions without disrupting the adsorbent framework.

The minimal performance loss suggests strong immobilization of nanoparticles within the biochar or supporting matrix, thereby reducing nanoparticle leaching and preventing agglomeration during repeated cycles [30]. Furthermore, the persistence of high removal efficiency indicates that key adsorption mechanisms—surface complexation, ion exchange, and electrostatic attraction remain largely unaffected by regeneration [30].

The slight decline in performance after multiple cycles may be attributed to partial pore blockage, minor loss of active functional groups, or incomplete desorption of strongly bound metal species.

3.7 Microbial Contamination Before and After Treatment

The results of microbial contamination and subsequent treatment of well water using iron(III) oxide (Fe_2O_3) and silver oxide (Ag_2O) *Chromolaena odorata* leaf biochar nanocomposites (Fe_2O_3-COLBN and Ag_2O-COLBN), respectively, indicate the remarkable antimicrobial potency of these nanomaterials.

3.7.1 Microbial Contamination Before Treatment

From Table 1, all nine water samples analyzed showed significant microbial contamination before treatment, with total colony counts ranging from 1.60×10^4 to 1.90×10^5 CFU/mL. The presence of bacteria such as *Escherichia coli*, *Staphylococcus spp.*, *Shigella spp.*, *Klebsiella spp.*, *Proteus spp.*, and *Pseudomonas spp.* indicates fecal contamination, poor sanitation, and high risk of waterborne diseases [31, 32].

Table 1 Colony counts of bacteria isolated from different water sources after treatment with nanocomposites.

Water Sample	Number of Colonies before treatment	CFU/mL	Micro-organisms Isolated	Number of Colonies after treatment with Fe_2O_3-COLBN	CFU/mL	Number of Colonies after treatment with Ag_2O-COLBN	CFU/mL
Onuebonyi junction well	19	3.8×10^4	*Proteus*	No growth	No growth	No growth	No growth
Ezzamgbo obodo permsite well	47	9.4×10^4	*Staphylococcus, Shigella*	No growth	No growth	No growth	No growth
Nwiboko compound Idembia Ishieke well	60	1.20×10^5	*E-coli, Shigella*	10	2.0×10^2	No growth	No growth
Omege well	8	1.60×10^4	*Staphylococcus*	No growth	No growth	No growth	No growth
Agbaja azumili well	12	2.4×10^4	*E-coli*	No growth	No growth	7	1.4×10^2
Best care hospital and maternity Ugwuachara well	95	1.90×10^5	*E-coli, staphylococcus*	No growth	No growth	No growth	No growth
Kpirikpiri market well	71	1.42×10^5	*E-coli, pseudomonas*	No growth	No growth	6	1.2×10^2
Azugwu junction well	11	2.2×10^4	*Staphylococcus, klebsiella, Shigella*	No growth	No growth	No growth	No growth
NO. 1, Orifite street well	21	4.2×10^4	*Klebsiella*	12	2.4×10^2	No growth	No growth

3.7.2 Effectiveness of Fe_2O_3-COLBN in Well Water Treatment

Treatment of the well water samples with Fe_2O_3-COLBN showed complete inhibition of microbial growth in seven of nine samples. Only two samples (Nwiboko compound and NO. 1, Orifite street) recorded residual bacterial counts of 2.0×10^2 and 2.4×10^2 CFU/mL, respectively, indicating more than 99% reduction in microbial load. It is believed that increased equilibration to 60 to 120 min could lead to complete removal of the microbial load. The generation of reactive oxygen species (ROS) by Fe_2O_3 nanoparticles, which disrupt microbial membranes and the adsorptive capacity of biochar, which helps trap and deactivate bacteria could be responsible for the antimicrobial activities [32].

3.7.3 Effectiveness of Ag_2O-COLBN in Well Water Treatment

The Ag_2O-COLBN was more effective in bacterial decimation, achieving 100% microbial inhibition in all samples except two (Agbaja Azumili and Kpirikpiri market), where microbial counts dropped to 1.4×10^2 and 1.2×10^2 CFU/mL, respectively. The effectiveness could be attributed to the broad-spectrum antimicrobial activity of silver oxide, which causes disruption of bacterial DNA replication and protein synthesis, penetration and destruction of microbial cell walls and membranes, and release of Ag^+ ions, which are toxic to bacterial cells even at low concentrations [33].

3.7.4 Morphological and Biochemical Test on Well Water

To further establish the nature of the microbes in the water samples, the antimicrobial treatment of well water using Fe_2O_3-COLBN and Ag_2O-COLBN was evaluated based on the presence and biochemical characteristics of bacterial isolates from different well water samples as shown in Table 2.

Table 2 Morphological and Biochemical Test on suspected microbes.

Sample	Suspected organism	Cell arrangement	Cell shape	Gram stain	Indole test	Oxidase test	Catalase test	Coagulase test	Citrate test	Methyl red test
Omege junction well	*staphylococcus*	Cluster	Cocci	+	+	-	-	-	+	-
Azugwu junction well water	*Klebsiella*	Single	Rod	-	+	-	+	-	+	+
Azugwu junction well water	*Shigella*	Single	Rod	-	+	-	+		-	-
Orifite Street well water	*Klebsiella*	Single	Rod	-	+	-	+		+	+
Kpirikpiri market well	*pseudomonas*	Single	Rod	-	+	-	+		+	-
Onuebonyi junction well water	*Proteus*	Single	Rod	-	+	+	+		+	+

3.7.5 Microbial Identification and Characterization Before Treatment

The untreated water samples from six different wells revealed the presence of various pathogenic bacterial species, identified through biochemical tests such as Gram staining, indole, oxidase, catalase, citrate, methyl red, and coagulase tests, and their characteristics are shown in Table 3.

Table 3 Characteristics of bacterial isolates.

Sample Location	Suspected Organism	Cell Arrangement	Cell Shape	Gram Stain	Pathogenic Traits
Omege Junction	*Staphylococcus*	Cluster	Cocci	Gram-positive	Catalase-positive, Indole and Coagulase-negative
Azugwu Junction	*Klebsiella* and *Shigella*	Single	Rod	Gram-negative	Citrate-positive (*Klebsiella*), MR-negative
Orifite Street	*Klebsiella*	Single	Rod	Gram-negative	Indole and Citrate-positive
Kpirikpiri Market	*Pseudomonas*	Single	Rod	Gram-negative	Oxidase and Citrate-positive
Onuebonyi Junction	*Proteus*	Single	Rod	Gram-negative	Catalase, Citrate, Indole-positive

These isolates are known to be opportunistic or enteric pathogens**,** indicating fecal contamination and poor water hygiene. Their presence in well water poses significant public health risks, particularly *Klebsiella*, *Shigella*, and *Proteus*, which are commonly implicated in urinary tract infections, diarrhea, and other gastrointestinal disorders [32]. The microbial response based on treatment is shown in Table 4 and illustrates the plausible mechanism underlying microbial deactivation and denaturation.

Table 4 Microbial response to nanocomposite treatment.

Organism	Observation	Deduction
Staphylococcus	Inhibited	Susceptible to Ag^+ ions and ROS
Klebsiella	Inhibited	Sensitive to oxidative stress and nanoparticle-mediated membrane damage
Shigella	Inhibited	Gram-negative rods are vulnerable to nanocomposite attack
Pseudomonas	Partially inhibited or reduced	Known for resistance, but Ag-based materials are usually effective
Proteus	Inhibited	Susceptible to oxidative and ionic mechanisms

Characterization of Biochar and Nanocomposites.

3.7.6 The FTIR of Biochar and Nanocomposites

The Fourier Transform Infrared (FTIR) spectroscopy analysis of *Chromolaena odorata* biochar (COB), iron(III) oxide-*Chromolaena odorata* leaf biochar nanocomposite (Fe_2O_3-COLBN), and silver-*Chromolena odorata* leaf biochar nanocomposite (Ag-COLBN) is shown in Figure 12. It gives the functional groups and molecular interactions operating in the structures of the biochar and nanocomposites. The observed bands and band shifts along with their respective assignments reveal the structural modifications that occur upon metal oxide incorporation into the biochar matrix.

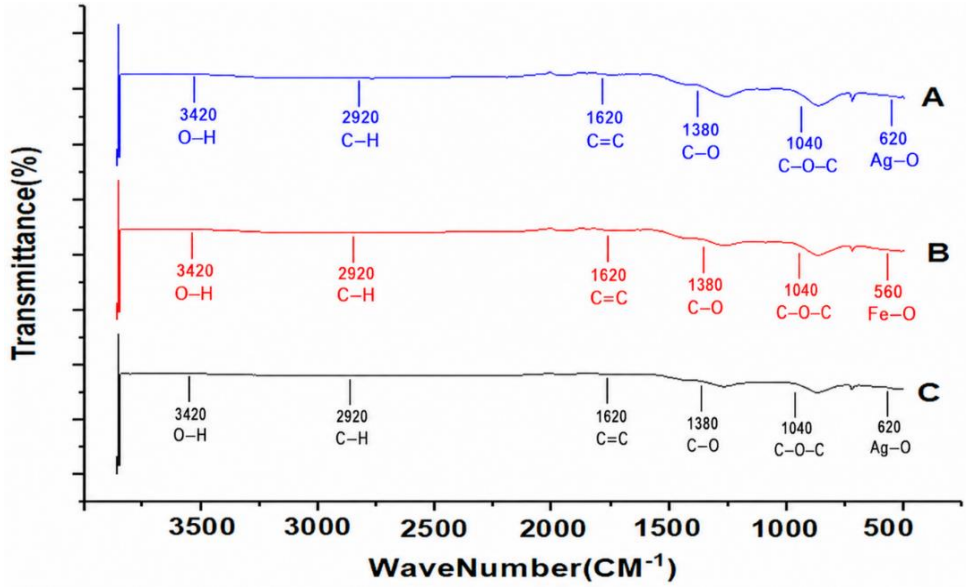

Figure 12 FTIR Vibration bands of COLB (C), Silver oxide *Chromolena odorata* leaf biochar nanocomposite (A), and iron(III) oxide *Chromolena odorata* leaf biochar nanocomposite (B).

The presence of broad bands around 3205.5 cm^{-1} (COB), 3224.1 cm^{-1} (Fe_2O_3-COLBN), and 3380.2 cm^{-1} (Ag-COLBN) indicates O-H stretching vibrations, attributed to hydroxyl groups from adsorbed

water, alcohols, or phenolic compounds. The C≡C stretching vibration at 2129.9–2120.9 cm^{-1} is common across all samples, indicating the presence of alkyne groups, possibly from lignocellulosic precursors of the biomass [22].

The C=O stretching bands shift from 1878.6 cm^{-1} (COB) to 1990.4 cm^{-1} in Fe_2O_3-COLBN and 2009.0 cm^{-1} in Ag-COLBN. This shift suggests interaction between the carbonyl groups and the embedded metal oxides, which may alter electron density and bonding environment [34]. The band at 1408.9 cm^{-1} in COB and Fe_2O_3-COLBN, and 1420.1 cm^{-1} in Ag-COLBN corresponds to C-H bending vibrations**,** indicating minor structural rearrangements due to silver nanoparticle loading.

A notable change was observed in the C-O stretching region, which shifts from 1244.9 cm^{-1} in COB to 1021.3 cm^{-1} in both nanocomposites, suggesting that C-O bonds in alcohols, phenols, or ethers were modified during metal nanoparticle intercalation, possibly due to surface oxidation or complexation [35]. The bands at 872.6–872.2 cm^{-1} across all samples correspond to C-H bending, confirming aromatic character in the biochar matrix. The Fe-O stretching vibration at 766.6 cm^{-1} in Ag-COLBN and 693.3 cm^{-1} in Fe_2O_3-COLBN confirms the successful incorporation of Ag_2O and Fe_2O_3 respectively into the biochar matrix [34].

3.7.7 SEM Analysis of Biochar and Nanocomposites

Scanning Electron Microscopy (SEM) of COLB (C), Silver Oxide-*Chromolaena odorata* Leaf Biochar Nanocomposite (A), and iron(III) Oxide-*Chromolaena odorata* Leaf Biochar Nanocomposite (B), as shown in Figure 13, provides detailed information about the surface morphology and texture of the studied materials and is crucial in evaluating how modifications or dopants affect matrix structures. The COB exhibits a relatively porous and less compact surface structure, which reflects the carbonaceous framework derived from the pyrolyzed plant material. This base structure is crucial as it provides the physical and chemical scaffold for nanocomposite formation and provides pore architecture for adsorption capacity but lacks the additional functionalities provided by metal oxide nanoparticles [35].

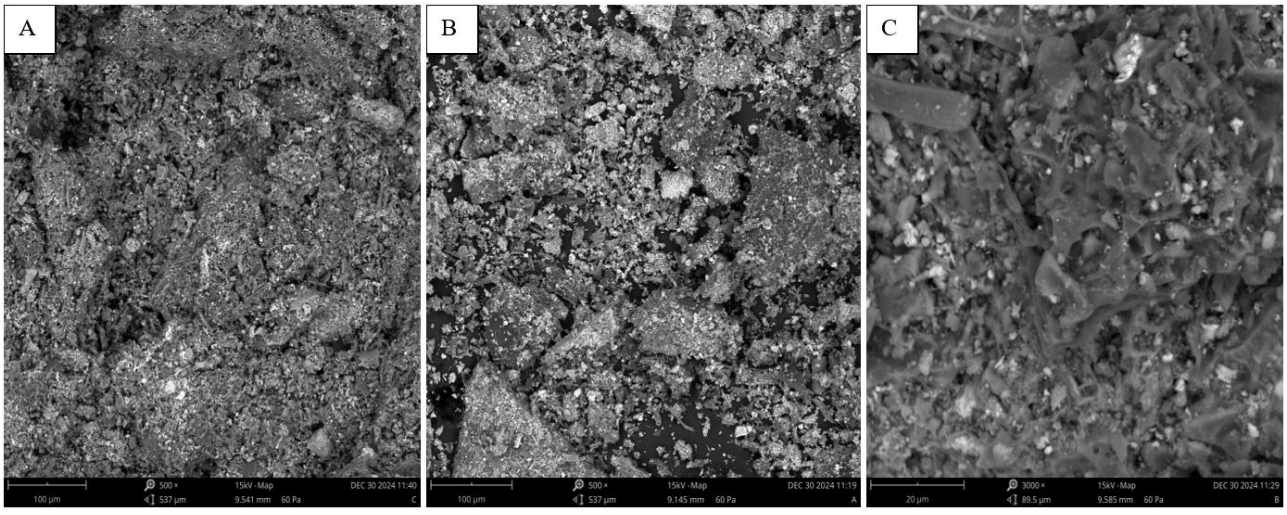

Figure 13 SEM micrograph of COLB (C), Silver oxide *Chromolena odorata* leaf biochar nanocomposite (A), and iron(III) oxide *Chromolena odorata* leaf biochar nanocomposite (B).

The SEM micrograph of Ag-COLBN likely reveals a rough and irregular surface with granular deposits, which are indicative of silver oxide nanoparticles well dispersed on the biochar matrix. These particles often appear as bright spots due to their higher electron density compared to the carbon matrix. The presence of Ag_2O nanoparticles enhances surface roughness and may increase the number of reactive sites, thereby improving photocatalytic and antimicrobial properties [36].

The SEM image of Fe-COLBN typically shows aggregated iron oxide particles embedded or anchored onto the porous biochar surface. The surface appears denser and less porous than Ag-COLB, possibly due to the sintering or agglomeration behavior of iron oxide nanoparticles. The iron particles contribute to magnetic and redox activity that are important in catalytic and adsorption applications [35]. The EDX elemental composition of the biochar and nanocomposites is presented in Table 5, Table 6, and Table 7. The presence of Fe and Ag in the nanocomposites of Table 6 and Table 7 respectively indicates that the actual incorporation of the metals into the biochar matrices.

Table 5 EDX of COLB.

Element Number	Element Symbol	Element Name	Atomic Conc.	Weight Conc.
20	Ca	Calcium	19.54	30.75
6	C	Carbon	36.24	17.09
19	K	Potassium	10.68	16.40
14	Si	Silicon	9.03	9.96
12	Mg	Magnesium	7.34	7.01
7	N	Nitrogen	9.55	5.25
15	P	Phosphorus	2.89	3.51
40	Zr	Zirconium	0.46	1.66
30	Zn	Zinc	0.62	1.59
26	Fe	Iron	0.68	1.49
29	Cu	Copper	0.56	1.39
38	Sr	Strontium	0.35	1.19
13	Al	Aluminium	1.00	1.06
25	Mn	Manganese	0.35	0.75
16	S	Sulfur	0.48	0.60
11	Na	Sodium	0.17	0.15
22	Ti	Titanium	0.07	0.13

Table 6 EDX of Fe_2O_3-COLBN.

Element Number	Element Symbol	Element Name	Atomic Conc.	Weight Conc.
6	C	Carbon	56.30	33.07
20	Ca	Calcium	14.98	29.37
14	Si	Silicon	6.46	8.87
12	Mg	Magnesium	5.60	6.66
26	Fe	Iron	2.33	6.37
7	N	Nitrogen	9.22	6.32
15	P	Phosphorus	2.37	3.59
13	Al	Aluminium	1.42	1.88
19	K	Potassium	0.79	1.51
38	Sr	Strontium	0.30	1.27
23	V	Vanadium	0.00	0.56
22	Ti	Titanium	0.23	0.53

Table 7 EDX of Ag_2O-COLBN.

Element Number	Element Symbol	Element Name	Atomic Conc.	Weight Conc.
108	Ag	Silver	4.39	29.19
20	Ca	Calcium	19.72	25.37
6	C	Carbon	52.98	20.43
14	Si	Silicon	7.59	6.84
12	Mg	Magnesium	6.95	5.43
15	P	Phosphorus	3.30	3.28
83	Bi	Bismuth	0.25	1.65
38	Sr	Strontium	0.49	1.37
13	Al	Aluminium	1.43	1.24
26	Fe	Iron	0.58	1.04
19	K	Potassium	0.69	0.86
40	Zr	Zirconium	0.29	0.85
29	Cu	Copper	0.41	0.84
28	Ni	Nickel	0.37	0.70
22	Ti	Titanium	0.31	0.47
23	V	Vanadium	0.27	0.44

3.7.8 XRD Analysis of Biochar and Nanocomposites

X-ray diffraction (XRD) analysis is vital for determining the crystallinity and phase composition of materials. The XRD patterns of the COLB (C), Fe_2O_3-COLBN (A) and Ag_2O-COLBN (B) are shown in Figure 14. The XRD pattern of COLB shows broad peaks centered around 2θ = 20-30°, indicating the amorphous or poorly crystalline structure of the biochar. This is characteristic of carbonaceous materials, with diffraction peaks attributed to the (002) plane of graphitic carbon [8, 13]. The broadness of these peaks confirms a disordered carbon structure, as expected given the heterogeneous composition of plant-derived biochar.

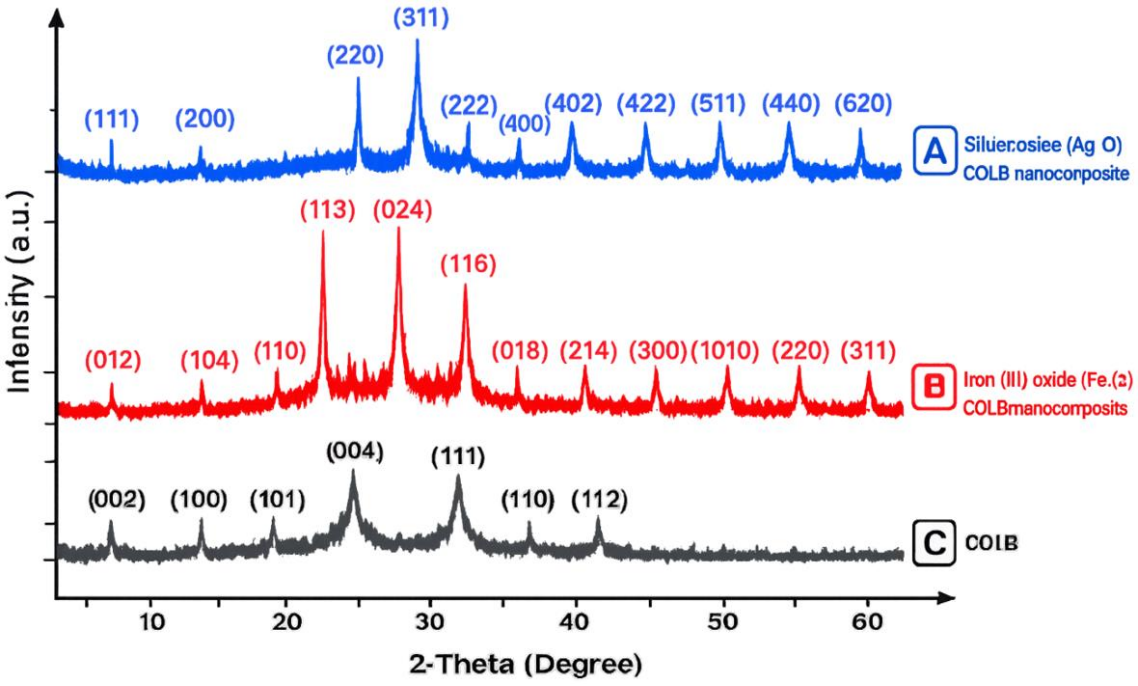

Figure 14 XRD Diffraction peaks of COLB (C), Silver oxide *Chromolena odorata* leaf biochar nanocomposite (A), and iron(III) oxide *Chromolena odorata* leaf biochar nanocomposite (B).

The incorporation of silver oxide nanoparticles onto COLB results in distinct diffraction peaks at 2θ values around 32.3°, 38.1°, 44.3°, 64.4°, and 77.4°, corresponding to the (111), (200), (220), (311), and (222) planes of Ag_2O and metallic Ag (JCPDS Card No. 04-0783 and 65-2871). The sharp peaks confirm the crystalline nature of the silver species and their successful deposition onto the biochar matrix [35].

The XRD pattern of the Fe_2O_3-COLB nanocomposite displays prominent peaks at 2θ ≈ 24.1°, 33.2°, 35.6°, 40.8°, 49.5°, 54.1°, and 62.5°, which are indexed to the (012), (104), (110), (113), (024), (116), and (214) planes of hematite α-Fe_2O_3 (JCPDS Card No. 33-0664). These sharp, well-defined peaks are characteristic of highly crystalline hematite nanoparticles embedded within the biochar matrix [10].

3.7.9 UV Analysis of Biochar and Nanocomposites

The UV-Vis absorption spectra of COLB (C), Fe_2O_3-COLBN (A) and Ag_2O-COLBN (B) is shown in Figure 15 and provide defined insight into the optical properties and surface plasmon resonance (SPR) characteristics of synthesized nanocomposites. There is no absorption peak in the UV-Vis spectrum of COLB, which could be attributed to its highly carbonized nature, a lack of chromophoric groups, or metal-based electronic transitions, and is in line with other studies [34]. From Figure 15, the absorption peak at 757.27 nm is characteristic of Ag_2O nanomaterials and suggests that the Ag_2O-*Chromolaena odorata* biochar nanocomposite has strong optical activity in the visible to NIR range [35].

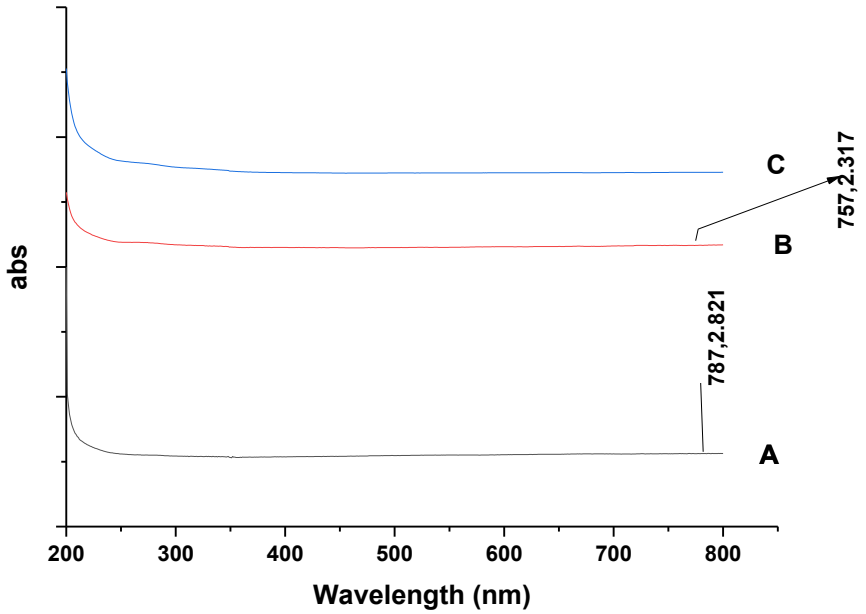

Figure 15 UV-vis of COLB (C), Silver oxide-*Chromolena odorata* leaf biochar nanocomposite (A), and iron(III) oxide-*Chromolena odorata* leaf biochar nanocomposite (B).

The absorption peak at 271.00 nm suggests the presence of Fe-O charge transfer transitions, commonly observed in iron-based nanocomposites [12]. This peak indicates that incorporating iron(III) oxide into *Chromolaena odorata* biochar enhances its optical response.

3.7.10 TEM Analysis of COLB (C), Fe_2O_3-COLBN (A) and Ag_2O-COLBN (B)

Transmission Electron Microscopy (TEM) micrographs of COLB (C), Fe_2O_3-COLBN (A) and Ag_2O-COLBN (B) are shown in Figure 16 and give detailed information on the morphology, size, and dispersion of nanoparticles in a composite. The histogram showing the particle size distribution of the biochar and nanocomposites is shown in Figure 17.

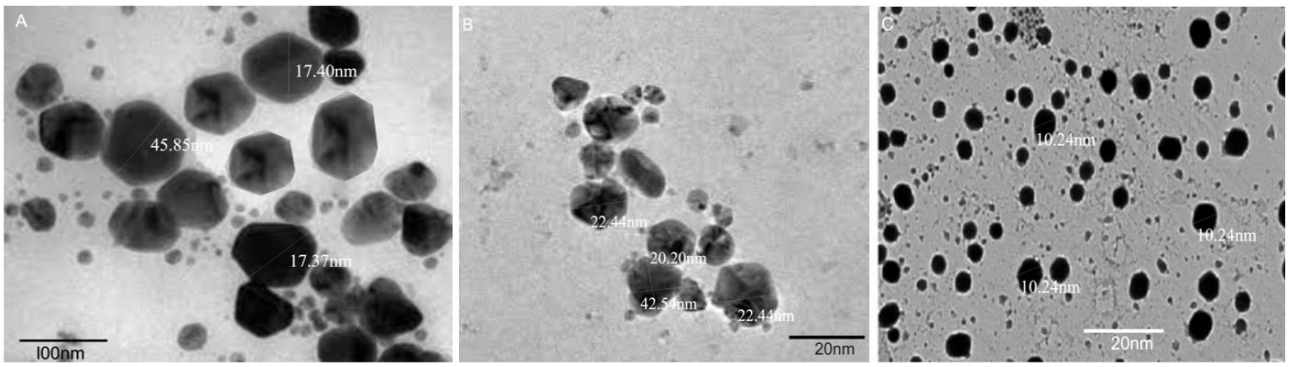

Figure 16 TEM micrograph of COLB (C), Silver oxide *Chromolena odorata* leaf biochar nanocomposite (A), and iron(III) oxide *Chromolena odorata* leaf biochar nanocomposite (B).

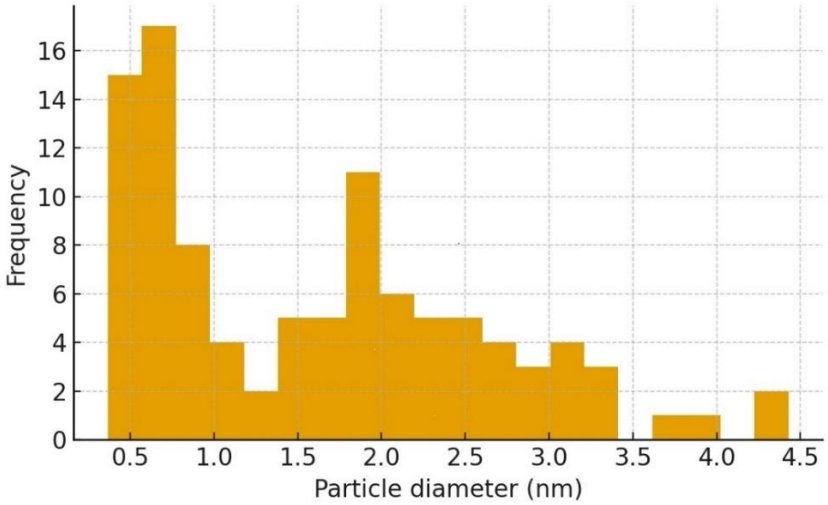

Figure 17 The histogram of the biochar and nanocomposites.

The TEM image of COLB reveals an amorphous and porous carbonaceous structurecharacteristic of biomass-derived biochar. The porous nature indicates a high surface area suitable for adsorption and nanocomposite loading [8]. The absence of distinct crystalline phases suggests that the biochar is mainly carbon-based and has low crystallinity. The TEM micrograph of the Ag-COLBN nanocomposite (A) shows well-dispersed, spherical-to-quasi-spherical silver oxide nanoparticles distributed on the biochar surface. These nanoparticles appear as darker-contrast regions due to their higher electron density compared to carbon. The particle size appears to range from approximately 10-30 nm, which aligns with typical dimensions reported in similar studies [8]. This uniform dispersion indicates effective incorporation of silver oxide onto the biochar matrix. In the case of Fe-COLBN (B), the TEM micrograph displays clusters of iron(III) oxide nanoparticles embedded within the biochar matrix. These nanoparticles are typically smaller (5-20 nm) and exhibit a more aggregated morphology than their silver counterpart. This aggregation could be due to the magnetic nature of iron oxide nanoparticles, which promotes particle-particle interactions [35].

The antimicrobial evaluation inhibitory effects of *Chromolaena odorata* leaf biochar (COLB), iron(III) oxide *Chromolaena odorata* leaf biochar nanocomposite (Fe-COLBN), and silver *Chromolaena odorata* leaf biochar nanocomposite (Ag-COLBN) against seven microorganisms: *Staphylococcus aureus*, *Escherichia coli*, *Klebsiella*, *Salmonella spp.*, *Candida albicans*, *Aspergillus spp.*, and *Proteus* are presented in Figure 18 and Plate 1. The COLB and Fe-COLBN both recorded a 12 mm zone of inhibition, while Ag-COLBN showed slightly lower activity (10 mm). This suggests that Fe-COLBN retains strong bactericidalactivity against Gram-positive bacteria, potentially due to oxidative stress induction and membrane disruption [23]. The Ag-COLBN demonstrated the highest inhibition (14 mm), followed by Fe-COLBN (12 mm) and COLB (10 mm). This reflects silver nanoparticles' well-documented efficacy against Gram-negative bacteria through silver ion release and reactive oxygen species (ROS) generation [23]. The Fe-COLBN and Ag-COLBN both exhibited 14 mm zones, surpassing COLB (12 mm). The equal performance of the two nanocomposites may be attributed to synergistic metal-biochar effects that enhance antimicrobial penetration and sustained ion release [22]. The Fe-COLBN achieved the highest inhibition (14 mm), with Ag-COLBN at 12 mm and COLB at 10 mm. The superior Fe-COLBN performance here could result from iron oxide nanoparticles' ability to generate hydroxyl radicals through Fenton-like reactions [21]. All three materials (COLB, Fe-COLBN, and Ag-COLBN) showed similar inhibition (10 mm), suggesting

moderate antifungal potential. This may be due to the inherent resistance of yeasts compared to bacteria [23]. The COLB showed the highest inhibition (10 mm), followed by Ag-COLBN (9 mm) and Fe-COLBN (8 mm). This indicates that metal nanoparticle incorporation did not significantly enhance antifungal activity against filamentous fungi in this case. All treatments showed identical inhibition (10 mm), implying that nanoparticle loading did not substantially improve efficacy against *Proteus*, possibly due to its intrinsic resistance mechanisms [22]. From Table 8, the MIC values revealed greater susceptibility of most microorganisms at 0.001 g/mL. In contrast, Aspergillus *spp.* and *Staphylococcus aureus* (for Fe-NC) required a higher concentration (0.010 g/mL), suggesting relatively greater resistance. Nevertheless, the inhibition zones produced by the nanocomposites remained significantly lower ($p < 0.05$) than those of the positive controls, indicating moderate but concentration-dependent antimicrobial efficacy.

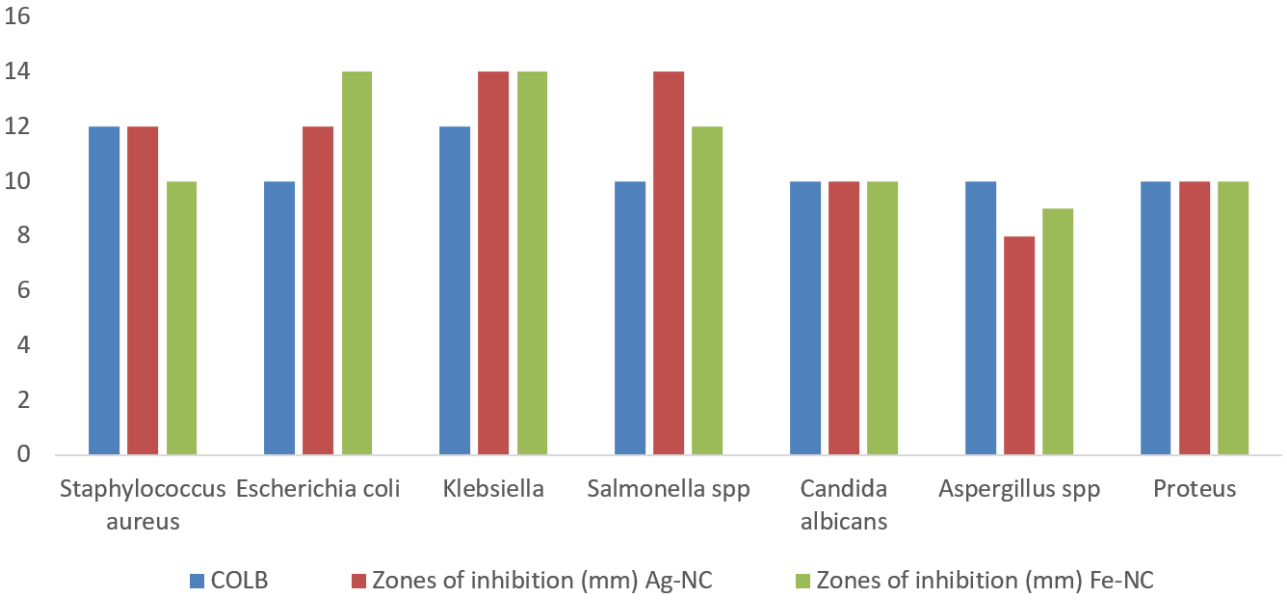

Figure 18 Antimicrobial (*Staphylococcus aureus*, *Escherichia coli*, *Klebsiella*, *Salmonella spp.*, *Candida albicans*, *Aspergillus spp.* and *Proteus*) evaluation of well water using COLB = blue, Ag-COLBN = Green and Fe-COLBN = Red.

Plate 1 Inhibition zone diameter of COLB, Ag-COLBN and Fe-COLBN.

Table 8 Antimicrobial (*Staphylococcus aureus*, *Escherichia coli*, *Klebsiella*, *Salmonella spp.*, *Candida albicans*, *Aspergillus spp.* and *Proteus*) evaluation of COLB, Ag-NC and Fe-NC and the MIC.

Microorganism	Compound	0.001 g/mL (mm)	0.01 g/mL (mm)	0.1 g/mL (mm)	Control (mm)	MIC (g/mL)
Staphylococcus aureus	COLB	8.00 ± 0.000 b	10.00 ± 0.001 b	12.00 ± 0.010 b	25.00 ± 0.000 a	0.001
	Ag-NC	9.00 ± 0.001 b	10.00 ± 0.015 b	12.00 ± 0.001 b	25.00 ± 0.001 a	0.001
	Fe-NC	6.00 ± 0.010 c	8.00 ± 0.001 c	10.00 ± 0.015 c	25.00 ± 0.001 a	0.010
Escherichia coli	COLB	6.00 ± 0.001 c	8.00 ± 0.010 c	10.00 ± 0.001 c	24.00 ± 0.000 a	0.010
	Ag-NC	8.00 ± 0.001 b	10.00 ± 0.001 b	12.00 ± 0.015 b	24.00 ± 0.001 a	0.001
	Fe-NC	10.00 ± 0.001 a	12.00 ± 0.010 a	14.00 ± 0.001 a	24.00 ± 0.015 a	0.001
Klebsiella	COLB	8.00 ± 0.001 b	10.00 ± 0.015 b	12.00 ± 0.001 b	24.00 ± 0.001 a	0.001
	Ag-NC	10.00 ± 0.001 a	12.00 ± 0.001 a	14.00 ± 0.010 a	24.00 ± 0.001 a	0.001
	Fe-NC	10.00 ± 0.001 a	12.00 ± 0.001 a	14.00 ± 0.001 a	24.00 ± 0.015 a	0.001
Salmonella spp.	COLB	6.00 ± 0.001 c	8.00 ± 0.001 c	10.00 ± 0.015 c	23.00 ± 0.000 a	0.001
	Ag-NC	10.00 ± 0.001 a	12.00 ± 0.010 a	14.00 ± 0.001 a	23.00 ± 0.001 a	0.001
	Fe-NC	8.00 ± 0.001 b	10.00 ± 0.001 b	12.00 ± 0.001 b	23.00 ± 0.015 a	0.001
Candida albicans	COLB	6.00 ± 0.001 b	8.00 ± 0.000 b	10.00 ± 0.001 b	20.00 ± 0.001 a	0.001
	Ag-NC	6.00 ± 0.001 b	8.00 ± 0.001 b	10.00 ± 0.010 b	20.00 ± 0.001 a	0.001
	Fe-NC	6.00 ± 0.000 b	8.00 ± 0.001 b	10.00 ± 0.001 b	20.00 ± 0.001 a	0.001
Aspergillus spp.	COLB	6.00 ± 0.001 b	8.00 ± 0.010 b	10.00 ± 0.001 b	18.00 ± 0.001 a	0.001
	Ag-NC	4.00 ± 0.001 c	6.00 ± 0.001 c	8.00 ± 0.015 c	18.00 ± 0.001 a	0.010
	Fe-NC	5.00 ± 0.010 c	7.00 ± 0.001 c	9.00 ± 0.001 c	18.00 ± 0.001 a	0.010
Proteus	COLB	6.00 ± 0.001 b	8.00 ± 0.001 b	10.00 ± 0.000 b	22.00 ± 0.001 a	0.001
	Ag-NC	6.00 ± 0.001 b	8.00 ± 0.010 b	10.00 ± 0.001 b	22.00 ± 0.001 a	0.001
	Fe-NC	6.00 ± 0.001 b	8.00 ± 0.001 b	10.00 ± 0.001 b	22.00 ± 0.000 a	0.001

4. Conclusion

This study, based on the results, has demonstrated that Ag-COLBN and Fe-COLBN are efficient, bio-inorganic materials for the treatment of well water. The nanocomposites show excellent adsorption and antimicrobial properties and effectively remove contaminants, including heavy metals, anions, and microorganisms. The nanocomposites are eco-friendly, easy to synthesize, can be used for multiple-cycle treatment of well water while maintaining stability, and as such are recommended for application in areas prone to water scarcity.

Acknowledgments

The authors are grateful to EBSU-TETFund Grant Ref No: EBSU/TETFund/IBR/2024/3 for financial support.

Author Contributions

Conceptualization: Felix Sunday Nworie; formal analysis: Felix Sunday Nworie, Chiamaka Mbam. Investigation: Felix Sunday Nworie and Ogonna Ogwa: writing—original draft preparation: Felix Sunday Nworie, and Nkechi Eze: visualization: Felix Sunday Nworie, Chiamaka Mbam; supervision: Felix Sunday Nworie and Ogonna Ogwa; project administration: Felix Sunday Nworie; Clinton Oroke, Chioma Ike-Elechi, Collins Chidiebere Igwe were involved in project management and have read and agreed to the manuscript be published in the journal.

Competing Interests

There is no competing interest in the publication of this journal.

AI-Assisted Technologies Statement

Artificial intelligence (AI) tools were used solely for basic grammar correction and language refinement in the preparation of this manuscript. Specifically, OpenAI's ChatGPT was employed to improve the readability and linguistic clarity of the English text. All scientific content, data interpretation, and conclusions were developed independently by the author. The authors have thoroughly reviewed and edited the AI-assisted text to ensure its accuracy and accept full responsibility for the content of the manuscript.

References

1. Youssef AM, El-Naggar ME, Malhat FM, El Sharkawi HM. Efficient removal of pesticides and heavy metals from wastewater and the antimicrobial activity of f-MWCNTs/PVA nanocomposite film. J Clean Prod. 2019; 206: 315-325.
2. Abdali N, Marjani A, Heidary F, Adimi M. Fabrication of PVA coated PES/PVDF nanocomposite membranes embedded with in situ formed magnetite nanoparticles for removal of metal ions from aqueous solutions. New J Chem. 2017; 41: 6405-6414.
3. Afiukwa JN, Afiukwa CA, Oti W. Determination of calcium, magnesium and total hardness concentrations in drinking water supply in Ebonyi State, Nigeria. Cont J Water Air Soil Pollut. 2012; 3: 12-16.

4. Ozoko DC. Geochemistry of natural water systems in Ugwulangwu, Ebonyi State, Nigeria. Int J Sci Res. 2015; 4: 3164-3169.
5. Ferreira D, Barros M, Oliveira CM, da Silva RJ. Quantification of the uncertainty of the visual detection of the end-point of a titration: Determination of total hardness in water. Microchem J. 2019; 146: 856-863.
6. Chidinma I, Matthew O, Grace E, Emmanuel N, Chika E, Ifeanyichukwu I, et al. Bacteriological and physicochemical parameters of some selected borehole water sources in Abakaliki metropolis, Nigeria. Int J Commun Med Public Health. 2016; 3: 3271-3277.
7. Spence K, Habibi Y, Dufresne A. Nanocellulose-based composites. In: Cellulose fibers: Bio-and nano-polymer composites. Berlin, Heidelberg: Springer Berlin Heidelberg; 2011. pp. 179-213.
8. Nworie FS, Nwabue FI, Oti W, Obasi C, Ejim C, Nwafor B. Synthesis of biochar conjugated Schiff base composites and their enhanced antimicrobial activity against five pathogenic organisms. Nova Biotechnol Chim. 2020; 19: 165-174.
9. Inyang CU, Adegoke AA. Antimicrobial properties and preliminary phytochemical screening of *Chromolaena odorata* (Siam or Sapysa weed) Leaf. Niger J Microbiol. 2008; 22: 1652-1659.
10. Opoku F, Kiarii EM, Govender PP, Mamo MA. Metal oxide polymer nanocomposites in water treatments. In: Descriptive inorganic chemistry researches of metal compounds. Norderstedt, Germany: BoD – Books on Demand; 2017. pp. 173-199.
11. Pandey N, Shukla SK, Singh NB. Water purification by polymer nanocomposites: An overview. Nanocomposites. 2017; 3: 47-66.
12. Nasir A, Masood F, Yasin T, Hameed A. Progress in polymeric nanocomposite membranes for wastewater treatment: Preparation, properties and applications. J Ind Eng Chem. 2019; 79: 29-40.
13. Yin J, Deng B. Polymer-matrix nanocomposite membranes for water treatment. J Membr Sci. 2015; 479: 256-275.
14. Eltaweil AS, Abdelfatah AM, Hosny M, Fawzy M. Novel biogenic synthesis of a Ag@Biochar nanocomposite as an antimicrobial agent and photocatalyst for methylene blue degradation. ACS Omega. 2022; 7: 8046-8059.
15. Naidoo KK, Coopoosamy RM, Naidoo G. Screening of *Chromolaeana odorata* (L.) King and Robinson for antibacterial and antifungal properties. J Med Plants Res. 2011; 5: 4859-4862.
16. Greenlee LF, Lawler DF, Freeman BD, Marrot B, Moulin P. Reverse osmosis desalination: Water sources, technology, and today's challenges. Water Res. 2009; 43: 2317-2348.
17. Shukla AK, Alam J, Ansari MA, Alhoshan M, Alam M, Kaushik A. Selective ion removal and antibacterial activity of silver-doped multi-walled carbon nanotube/polyphenylsulfone nanocomposite membranes. Mater Chem Phys. 2019; 233: 102-112.
18. Allah MA, Ibrahim HK, Abdulridha AA. Eco-friendly synthesis of ZnO/chitosan nanocomposite: Detailed characterization, DFT study, docking study, adsorption kinetics, thermodynamic analysis and antioxidant properties. J Mol Liq. 2025; 425: 127216.
19. Aktar P, Moonajilin MS. Assessment of water quality status of Turag River due to industrial effluent. Int J Eng Inf Syst. 2017; 1: 105-118.
20. Barakat A, El Baghdadi M, Rais J, Aghezzaf B, Slassi M. Assessment of spatial and seasonal water quality variation of Oum Er Rbia River (Morocco) using multivariate statistical techniques. Int Soil Water Conserv Res. 2016; 4: 284-292.

21. Hoseinzadeh E, Makhdoumi P, Taha P, Hossini H, Stelling J, Amjad Kamal M, et al. A review on nano-antimicrobials: Metal nanoparticles, methods and mechanisms. Curr Drug Metab. 2017; 18: 120-128.
22. Ghosh M, Mandal S, Roy A, Paladhi A, Mondal P, Hira SK, et al. Synthesis and characterization of a novel drug conjugated copper-silver-titanium oxide nanocomposite with enhanced antibacterial activity. J Drug Delivery Sci Technol. 2021; 62: 102384.
23. Kshatri J, Rao CV, Settaluri VS. Study of water quality and biochemical characterization of bacterial isolates from water samples of Ponnagi area in Krishna district. Biosci Biotechnol Res Asia. 2017; 14: 1129-1134.
24. Padmavathi P, Sunitha K, Veeraiah K. Efficacy of probiotics in improving water quality and bacterial flora in fish ponds. Afr J Microbiol Res. 2012; 6: 7471-7478.
25. Du J, Zhang L, Liu T, Xiao R, Li R, Guo D, et al. Thermal conversion of a promising phytoremediation plant (*Symphytum officinale L.*) into biochar: Dynamic of potentially toxic elements and environmental acceptability assessment of the biochar. Bioresour Technol. 2019; 274: 73-82.
26. Fong WM, Affam AC, Chung WC. Synthesis of Ag/Fe/CAC for colour and COD removal from methylene blue dye wastewater. Int J Environ Sci Technol. 2020; 17: 3485-3494.
27. Dehbi A, Dehmani Y, Omari H, Lammini A, Elazhari K, Abdallaoui A. Hematite iron oxide nanoparticles (α-Fe_2O_3): Synthesis and modelling adsorption of malachite green. J Environ Chem Eng. 2020; 8: 103394.
28. Chen B, Zhou D, Zhu L. Transitional adsorption and partition of nonpolar and polar aromatic contaminants by biochars of pine needles with different pyrolytic temperatures. Environ Sci Technol. 2008; 42: 5137-5143.
29. Ahmad M, Rajapaksha AU, Lim JE, Zhang M, Bolan N, Mohan D, et al. Biochar as a sorbent for contaminant management in soil and water: A review. Chemosphere. 2014; 99: 19-33.
30. Afkari M, Masoudpanah SM, Hasheminiasari M, Alamolhoda S. Effects of iron oxide contents on photocatalytic performance of nanocomposites based on g-C_3N_4. Sci Rep. 2023; 13: 6203.
31. Panchal P, Paul DR, Sharma A, Choudhary P, Meena P, Nehra SP. Biogenic mediated Ag/ZnO nanocomposites for photocatalytic and antibacterial activities towards disinfection of water. J Colloid Interface Sci. 2020; 563: 370-380.
32. Baral SC, Maneesha P, Datta S, Dukiya K, Sasmal D, Samantaray KS, et al. Enhanced photocatalytic degradation of organic pollutants in water using copper oxide (CuO) nanosheets for environmental application. JCIS Open. 2024; 13: 100102.
33. Seling TR, Katzbaer RR, Thompson KL, Aksoy SE, Chitara B, Shringi AK, et al. Transition metal-doped CuO nanosheets for enhanced visible-light photocatalysis. J Photochem Photobiol A. 2024; 448: 115356.
34. Chausali N, Saxena J, Prasad R. Nanobiochar and biochar based nanocomposites: Advances and applications. J Agric Food Res. 2021; 5: 100191.
35. Chapman HD, Pratt PF. Methods of analysis for soils, plants and waters. Soil Sci. 1962; 93: 68.
36. Chen WH, Huang JR, Lin CH, Huang CP. Catalytic degradation of chlorpheniramine over GO-Fe_3O_4 in the presence of H_2O_2 in water: The synergistic effect of adsorption. Sci Total Environ. 2020; 736: 139468.